SPATIOTEMPORAL ORGANIZATION, REGULATION AND FUNCTION OF TRACTION DURING NEUTROPHIL CHEMOTAXIS

BY

MYUNG EUN SHIN

DISSERTATION

Submitted in partial fulfillment of the requirements
for the degree of Doctor of Philosophy in Cell and Developmental Biology
in the Graduate College of the
University of Illinois at Urbana-Champaign, 2011

Urbana, Illinois

Doctoral Committee:

Professor Andrew S. Belmont, Chair
Assistant Professor Fei Wang, Director of Research
Professor Jie Chen
Associate Professor Phillip A. Newmark
Assistant Professor Yang Kevin Xiang

ABSTRACT

Despite recent advances in our understanding of biochemical regulation of neutrophil chemotaxis, little is known about how mechanical factors control neutrophils' persistent polarity and rapid motility. Here, by using a human neutrophil-like cell line and human primary neutrophils, we describe a dynamic spatiotemporal pattern of tractions in neutrophils during chemotaxis. Tractions are located at both the leading and the trailing edge of neutrophils, where they oscillate with a defined periodicity. Interestingly, traction oscillations at the leading and the trailing edge are out of phase with the tractions at the front leading those at the back, suggesting a temporal mechanism that coordinates leading edge and trailing edge activities. The magnitude and periodicity of tractions depend upon the activity of non-muscle myosin IIA. Specifically, traction development at the leading edge requires myosin light chain kinase (MLCK)-mediated myosin II contractility and is necessary for α5β1-integrin activation and leading edge adhesion. Localized myosin II activation induced by spatially activated small GTPase Rho and its downstream kinase p160-ROCK, as previously reported, leads to contraction of actin-myosin II complexes at the trailing edge, causing it to de-adhere. Our data identify a key biomechanical mechanism for persistent cell polarity and motility.

To my mother, Kwang Bok Jang, for her unconditional love and inspirations.

To my father, Dong Ryung Shin, for his steady love and support.

To my dearest friends along the way.

ACKNOWLEDGMENTS

My deepest gratitude goes to my advisor, Dr. Fei Wang for giving excellent guidance to me all these years and for always encouraging me to be a passionate scientist. Many thanks to my collaborators, especially Dr. Ning Wang, Dr. Martin Schwartz, Dr. Sungsoo Na, Dr. Farhan Chowdhury and Yeh-Chuin Poh for not only providing the reagents and the technical support, but for sharing their insights and excitement regarding my project. Thanks to all the past and present members of the Wang Lab for discussion and help with various aspects of my work. Also thanks to my committee members, Drs. Andrew Belmont, Jie Chen, Phillip Newmark, and Yang Kevin Xiang for their insightful questions and advice.

TABLE OF CONTENTS

CHAPTER 1

INTRODUCTION

Cell migration is a fundamental process associated with various biological and pathophysiological phenomena. Cell migration is conceptualized as a multi-step, cyclic process and can be broadly classified into two categories, i.e., mesenchymal and amoeboid migration. It is the latter category that neutrophil chemotaxis falls under.

Chemotaxis – the directed movement of cells in a gradient of chemoattractant – is essential for neutrophils to crawl to sites of inflammation and infection. Chemoattractant-induced activation of spatially localized cellular signals causes neutrophils to initiate polymerization of actin at the leading edge (pseudopod), polarize (i.e., adopt an asymmetric shape with defined front and back) and move towards the highest concentration of the chemoattractant. Recent studies have begun to reveal some fascinating details of the intracellular biochemical components that spatially direct the neutrophils' cytoskeleton and the complex signaling pathways that control formation of their front and back.

Despite these findings, there are significant gaps in our understanding of the mechanical functions that control the persistent and rapid movement of neutrophils. Specifically, there is limited documentation of quantitative analysis of tractions in neutrophils, and the spatial and temporal dynamics, regulation and functions of tractions remain largely undefined.

Cell migration is a multi-step, cyclic process

Cell migration is a universal process that most cells in the body undergo at a given time and tissue space (Friedl, 2004). Therefore, it is widely involved in numerous biological as well as pathophysiological processes such as embryonic morphogenesis, tissue repair and regeneration, disease progression in cancer, mental retardation, and arthritis (Ridley et al., 2003). In general, cell migration is conceptualized as a multi-step, cyclic process. Initially, a cell will respond to a migration-promoting agent by polarizing and extending protrusions in the direction of migration. These protrusions are usually

driven by actin polymerization, can take a form of large, broad lamellipodia or small, spiky filopodia, and are stabilized by adhering to the extracellular matrix (ECM) or adjacent cells via transmembrane proteins linked to actin cytoskeleton (adhesion). These adhesions provide traction for migration as the cell propels its cytoplasmic body over them, and they are disassembled (de-adhesion) at the cell rear, leading to detachment (tail retraction). A migration cycle is completed at this point. The cell initiates another cycle of migration with protrusion, followed again by adhesion, de-adhesion and tail retraction, and repeats this multi-step process until it arrives at its target location.

Mesenchymal and amoeboid migration

While many aspects of migration are shared among different cell types, the details can be greatly varied. As of present, a single cell migration (as opposed to collective cell migration) is broadly classified into two modes, that is, mesenchymal migration and amoeboid migration. In the following, I discuss the distinct features of two such modes of migration.

Slow-moving mesenchymal cells such as fibroblasts, myoblasts, single endothelial cells, and sarcoma cells exhibit distinct steps in the migration cycle as described in the previous section. Mesenchymal cells typically adopt a spindle-shaped, elongated morphology (Grinnell, 1994; Tamariz and Grinnell, 2002), which is dependent upon integrin-mediated adhesion dynamics and the presence of high traction forces on both cell poles (Ballestrem et al., 2001; Tamariz and Grinnell, 2002). Blocking integrins in fibroblasts, endothelial cells or tumor cells with antibody or small-molecule inhibitors induces cell retraction, acquisition of spherical shape and impaired migration (Friedl, 2004). Concomitant to integrin and actin focalization at substrate-binding sites (termed focal adhesions or focal contacts), mesenchymal cells recruit surface proteases to digest and remodel the ECM (Wolf et al., 2003a). Focal contact formation and turnover occur in the timescale of 10~120 minutes, resulting in relatively slow migration velocities (0.1-2 μm/min) (Ballestrem et al., 2001; Peter Friedl, 1998; W. Matthew Petroll, 2003; Zamir et al., 2000).

In contrast, in fast-crawling amoeboid cells, such as neutrophils or more primitive *Dictyostelium discoideum*, steps in the migration cycle are less obvious: these cells seem

to glide over the substratum. In response to migration-promoting agents, amoeboid cells rapidly adopt a highly polarized shape, which is generated by cortical filamentous actin that mediates cell dynamics as well as providing stiffness to the cell body. Also, other amoeboid cells, including T lymphocytes and some metastatic tumor cells, usually use protease-independent physical mechanisms to overcome matrix barriers including adaptation of the cell-shape change to preformed matrix structures and squeezing through narrow spaces (Wolf et al., 2003b). Interestingly, unlike mesenchymal cells, no stable focal contacts (and stress fibers) are detected within leukocytes, whereas fast and non-focalized receptor assemblies at cell-substrate interactions are retained (Peter Friedl, 1998; Wolf et al., 2003b). This lack of stable focal contacts and proteolysis is thought to allow these cells to turn over membrane rapidly and move at high velocities (2-30 μm/min) (Peter Friedl, 1998).

Neutrophil chemotaxis is an important mechanism of an innate immune system against invading pathogens

Polymorphonuclear neutrophils (PMN) are one of the first cells to reach the site of bacterial or viral infection and thus provide a critical first line of defense in the immune system against invading pathogens. At the same time, neutrophil-mediated tissue injuries in a number of inflammatory or autoimmune diseases such as acute respiratory distress syndrome (ARDS), post ischemic injury and arthritis can be detrimental. Therefore, more thorough understanding of mechanism of neutrophil chmotaxis is important as it may not only expand our knowledge of cell migration in general, but also facilitate development of therapeutic technologies against such diseases.

Upon infection or inflammation, neutrophils circulating in the bloodstream are recruited to the injured tissue in a coordinated series of steps, which are, broadly speaking, capturing (tethering), rolling, arrest, crawling, transendothelial migration and interstitial migration (Zarbock and Ley, 2009). Neutrophils are first ‘captured’ by the inflamed blood endothelium, the process mediated by selectins and their counter-receptors expressed on both cell types (Kansas, 1996). Captured neutrophils start to ‘roll’ on the endothelium through the action of selectins and integrins. As neutrophils encounter chemoattractants presented on the endothelial cell surface, cells become ‘arrested’ by the

strengthening of the intercellular adhesion between neutrophils and endothelium. At this point, neutrophils adopt a highly polarized fan-shaped morphology and begin to crawl on the endothelium. Cells eventually exit the blood vessels, crawling through an endothelium (transendothelial migration) and continuing to migrate through an interstitium to the target location (interstitial migration).

Biochemical signaling pathways underlying neutrophil polarity

Chemotaxis is defined as a directed movement up a gradient of chemoattractant. Strictly adhering to such definition, neutrophil chemotaxis would be further limited to the steps following the arrest in the aforementioned neutrophil recruitment cascade, namely crawling, transendothelial migration and interstitial migration, as these steps directly involve interpretation of external chemical gradient by cells. To avoid confusion in the discussion hereafter, I refer to the crawling of neutrophils on a two-dimensional surface as neutrophil chemotaxis, unless noted otherwise.

One striking feature of neutrophil chemotaxis is the ability of cells to interpret shallow gradients of external attractant to generate morphological polarity. In fact, it is a characteristic shared by most chemotactic cells, including *Dictyostelium discoideum* and fibroblasts, albeit with different degrees. In particular, upon exposure to chemoattractants, amoeboid neutrophils rapidly adopt a polarized morphology in which filamentous actin (F-actin) is predominantly recruited to the leading edge. In addition, actomyosin contractile complexes are found both at the leading edge and trailing edge in neutrophils, with the majority of complexes localized at the trailing edge. Such spatial segregation of distinct actin assemblies is thought to account for morphological polarity of neutrophils, in which propulsion of F-actin against the plasma membrane at the leading edge leads to a broad front, whereas contraction of actomyosin complexes at the trailing edge results in a narrow back. Surprisingly, a gradient of chemoattractant is not necessary for neutrophils to polarize: in uniform concentration of chemoattractant, neutrophils can polarize, albeit in random directions and with reduced persistency.

How do neutrophils polarize? Studies on primary human neutrophils mostly relied on pharmacological inhibitors due to two properties of these cells; they are terminally differentiated cells and die within 24 hrs after isolation from the blood, and are refractory

to transfection. Such challenges in studying human neutrophils have been overcome recently by the development of a culture model of human neutrophils. HL-60 is a cell line derived from promyelocytic leukemia cells which can be differentiated by DMSO to have neutrophil-like properties and are genetically tractable (Hauert et al., 2002). With this model system, the following model of biochemical signaling pathways underlying polarity of human neutrophils emerged.

A frontness signaling pathway involving positive feedback loop of PI3K, Rac, and F-actin

The first step toward understanding signals involved in the positive feedback loop was the demonstration that phosphatidylinositol-3,4,5-tri-phosphate (PI[3,4,5]P3) and other products of phophoinositide-3'-kinase (PI3Ks) accumulate selectively in membranes of the moving cell's leading edge in *Dictyostelium* (Meili and Firtel, 2003; Parent, 2004; Parent et al., 1998) and neutrophil-like HL-60 cell line (Servant et al., 2000; Wang et al., 2002). These PI3Ps are critical in organizing the neutrophil's leading edge, as shown by experiments in which pharmacologic inhibitors of PI3Ks block attractant-stimulated formation of actin polymers and pseudopods (Servant et al., 2000; Wang et al., 2002) by abrogating activation of small GTPases of the Rho family, including Rac and Cdc42 (Benard et al., 1999), which are known to promote formation of actin polymers (Ridley, 2001; Tapon and Hall, 1997). It has been shown recently by several groups (Srinivasan et al., 2003; Wang et al., 2002; Weiner et al., 2002) that PI3Ps and Rac serve as signals in a positive feedback loop that organizes the leading edge of HL-60 cells. While PI3Ps are required for activation of Rac, the reverse is also true: inhibiting Rac activation (with toxins or a dominant negative Rac mutant) prevents PI3P accumulation (Servant et al., 2000; Srinivasan et al., 2003; Wang et al., 2002). Furthermore, addition of exogenous PI(3,4,5)P3 can trigger the positive feedback loop directly, initiating accumulation of endogenous PI3Ps (Weiner et al., 2002), morphologic polarity, and motility in the absence of added chemoattractant (Verena, 2000; Weiner et al., 2002). These effects are completely blocked by PI3K inhibitors and toxins that inhibit activation of Rho GTPases, indicating that they depend on activation of both endogenous PI3P synthesis and Rac by the exogenous lipid. Finally, Rac stimulates PI3P accumulation, at least in part, via actin polymers that are generated in response to

activated Rac: either attractant or expression of constitutively active Rac can trigger persistent PI3P accumulation, but both effects are prevented when actin polymerization is blocked by latrunculin B, which sequesters actin monomers (Srinivasan et al., 2003; Wang et al., 2002). Finally, inactivation of Gi by pertussis toxin (PTX) abrogates frontness responses tested in neutrophils and differentiated HL-60 cells, including polymerization of actin, activation of Rac and Cdc42, and PI3P-dependent phosphorylation of Akt, although cell's ability to form uropod was left intact (Wang et al., 2002). In conclusion, the model for frontness in which activation of Gi triggers the feedback loop of PI3K, Rac, and F-actin explains the persistence of robust actin and PI3P-containing pseudopods during neutrophil chemotaxis.

A backness signaling pathway suggests a model for neutrophil self-organizing polarity

Previous studies suggest that in addition to the frontness signals, attractant receptors trigger a backness pathway that contributes to polarity: In contrast to the frontness pathway, which is triggered by Gi, the backness signaling pathway is initiated by G12 and G13 (Xu et al., 2003). Their downstream components include a Rho, a Rho-dependent protein kinase (p160-ROCK), and activated myosin, which results in contraction of actomyosin complexes at the cell membranes at the trailing edge. At each step of the pathway the corresponding constitutively active mutants induced a global backness response: cells rounded up and failed to form actin polymers or recruit PH-AKT-GFP (the PH domain of protein kinase Akt fused to GFP, used as a spatial probe for 3′-phosphoinositol lipids) to the leading edge in response to fMLP, but instead accumulated activated myosin around the entire cell periphery. Conversely, inhibiting each of these steps with pharmacological drugs or dominant negative mutants impaired cell contractility at the back and caused cells to form an elongated tail. Myosin II-mediated contractility is also involved in reducing the sensitivity of the back of the cells because abrogating the backness pathway renders the entire cell sensitive to fMLP stimulation and generates multiple pseudopods (Xu et al., 2003).

This model explains, at least partially, how a neutrophil responding to fMLP adopts morphological polarity. From the receptor level, two divergent pathways involving distinct molecules are generated to induce actin polymerization and actin-

myosin assemblies, respectively. Spatial segregation between these two actin assemblies in the membrane is possible due to mutual inhibition between these assemblies. Such mutual incompatibility and inhibition between frontness and backness may account for the ability of neutrophils and HL-60 cells to polarize in uniform concentrations of chemoattractant and to perform U-turns rather than simply reverse polarity in response to changes in the direction of the attractant gradient. The neutrophil follows its sensitive nose because positive feedback loops at the front and Rho/myosin-mediated contraction (inhibition) at the back render the pseudopod much more sensitive to PI3P- and Rac-activating actions of the attractants (Xu et al., 2003).

It is important to note that while the model has facilitated our understanding of how polarity occurs in neutrophil chemotaxis, it is not without limitations. It does not address the spatiotemporal dynamics of the activation of the two distinct pathways in neutrophils responding initially to chemoattractants in gradients; rather, it explains the polarity on the premise that both pathways are simultaneously active. Thus, the picture is unclear whether there is a temporal difference in the initial activation of two distinct pathways in response to the chemoattractants leading to the spatial segregation of two pathways within neutrophils. Future experiments addressing the precise spatiotemporal dynamics of the activities of the frontness and backness pathways will allow one to draw a more complete picture of polarity in neutrophil chemotaxis. For instance, in one speculative model following this idea, graded activation of one pathway (presumably the frontness pathway) corresponding to the extracellular chemoattractant gradient occurs prior to the activation of the other pathway, thereby preoccupying a portion within cells. The delayed activation of the other pathway (presumably the backness pathway) may follow, and because of the mutual inhibition between the two pathways, its signals may be limited to the cellular region where the first signal is relatively weak.

Mechanical regulations in neutrophil chemotaxis are poorly understood

While various biochemical regulatory mechanisms controlling neutrophil chemotaxis have been studied extensively, mechanical regulation that governs the persistent and rapid movement of neutrophils remains poorly understood. In particular, there is limited documentation of quantitative analysis of tractions in neutrophils. At the

time the thesis was conceived, only a single study (Smith et al., 2007) was available concerning measurement of traction during neutrophil chemotaxis. Though valuable, the study was limited in that the temporal resolution was inadequate (traction measurement interval of 1-2 minutes) to fully capture the traction dynamics occurring in fast migrating neutrophils and that the substrate stiffness used was much higher than what neutrophils normally encounter in physiological settings. Thus, the spatial and temporal dynamics, regulation and functions of tractions remain largely undefined and required a thorough examination.

Traction in cell migration

Why is traction important in motile cells? Cells crawling on two dimensional surfaces interact with their environment not only biochemically but also mechanically. In particular, the latter mode of interaction is thought to provide driving force for motile cells; in order to move forward, cells need to exert rearward traction forces (Dembo and Wang, 1999; Lauffenburger and Horwitz, 1996; Oliver, 1994).

Current knowledge on traction in motile cells is mostly based on studies using slow moving cells such as fibroblasts. These cells show prominent adhesion structures with a relatively slow turnover rate, which can serve as robust anchorage sites between cell and extracellular matrix (ECM) and transmit the traction forces. In addition, relatively low time resolution required to capture the traction dynamics rendered these slow migrating cells a preferable choice to study than their fast moving counterparts.

In slow migrating cells such as fibroblasts, tractions are broadly organized into two distinct zones. In the lamellipodial region, large centripetal tractions are found along the periphery of the cells, which get countered by tractions developing at the lamellipodia-lamella border (Munevar, 2001). In marked contrast, the trailing edge contains only a few isolated spots of weak tractions which are in parallel with the overall direction of cell motility. Such front-to-back asymmetry in traction pattern agrees well with the frontal towing model (Beningo and Wang, 2002; Dembo and Wang, 1999; DiMilla et al., 1991; Munevar, 2001). The model is based on the idea of differential adhesion strengths in motile cells, i.e., front adhesions are strong whereas the back adhesions are weak. In this model, contraction of actin cytoskeleton causes tension to be

transmitted to those two classes of adhesion, pulling the front adhesions rearward and pushing the back adhesions forward. Relatively strong adhesions at the leading edge withstand such backward pulling force and provide counter force to cells to move forward. In contrast, the relatively weak adhesions at the trailing edge are dissociated upon force transmission, causing the cytosolic flow and protrusion of front membrane.

While tractions provide slow migrating cells with driving force at the cellular level, it functions to facilitate the strengthening of nascent leading-edge adhesions at the molecular level (Balaban et al., 2001). Slow moving cells such as fibroblasts assemble transient adhesions called focal complexes at the leading edge, which mature into more stable focal adhesions (Rottner et al., 1999). Development of focal adhesions is essential for persistent protrusion of lamellipodia, as focal adhesions provide robust anchors to the extracellular matrix (ECM), allowing actomyosin contractile forces to pull the cell body forward without detachment from ECM. In agreement with this, persistent traction spots at the leading edge correlate well with both the development of further protrusion and the direction of overall cell migration (Munevar, 2001).

In fast migrating cells such as *Dictyostelium discoideum,* the asymmetrical distribution of tractions – yet, a reversed one compared to that of fibroblasts - has been reported, with higher traction in the rear and lower traction at the front (Lombardi et al., 2007). Such asymmetry in traction has led some to hypothesize a model in which the rear contraction or squeezing induces the dissociation of back adhesions as well as driving a forward cytoplasmic flow and protrusion of the lamellipodia (Condeelis, 1993; Yanai, 2004; Yanai, 1996). However, the pattern, regulation and functions of traction in neutrophil chemotaxis need more thorough examination as mentioned above.

CHAPTER 2

SPATIOTEMPORAL ORGANIZATION OF TRACTIONS DURING NEUTROPHIL CHEMOTAXIS

Introduction

As discussed in the Chapter 1, traction in neutrophil chemotaxis has not been examined in a rigorous fashion, thus requiring a careful analysis. In this chapter, I address the spatiotemporal pattern of traction during neutrophil chemotaxis. Highly dynamic tractions are found in both leading and trailing edges of neutrophils during chemotaxis. Tractions at both edges oscillate periodically with a time offset.

Materials and methods[1]

Isolation of primary neutrophils and HL-60 cell culture

Primary neutrophils were isolated from venous blood from healthy human donors. Blood was collected into heparin-containing Vacutainer tubes (BD Biosciences) and neutrophil isolation procedure was performed within 30 min of blood collection using PMN isolation medium (Matrix). Red blood cell contaminants were removed by Red Blood Cell Lysis buffer (Roche), producing more than 97% of neutrophil purity. Neutrophils were suspended in RPMI 1640 medium supplemented with 10% fetal bovine serum at 37°C until the time of experiments conducted within 8 h after isolation.

Cultivation and differentiation of HL-60 cells were as described (Wang et al., 2002).

Polyacrylamide gel substrates, traction force microscopy (TFM) and data analysis

Polyacrylamide gels were prepared as described (Pelham and Wang, 1999). Red fluorescent microspheres (0.2 μm, Molecular Pobes) were embedded in gels for traction detection, and the gels were coated with 10 μg/ml human fibronectin. The elastic Young modulus of the polyacrylamide gels was 3.5 kPa (5% acrylamide; 0.10% bis-acrylamide)

[1] In the case of a method concerning multiple chapters, the explanation was given only once in the first chapter the given method appears.

(Engler et al., 2004; Tolic-Norrelykke et al., 2002) . 100 kPa gels, were generated as described by Oakes *et al* (Oakes et al., 2009). Briefly, dHL-60 cells or primary neutrophils (1.0×10^5) with or without various treatments were allowed to adhere to the fibronectin-coated polyacrylamide gel for 10 min at 37°C and migrate toward the micropipette containing 10 μM fMLP for 5 min. Traction force microscopy was performed using Andor Technology Revolution System Spinning Disk Confocal Microscopy system (Andor) coupled to an Olympus IX71 inverted microscope with Olympus 100x APO/1.4 NA objective. The working distance of the objective is ~0.13 mm, which far exceeds the thickness of the polyacrylamide gel (75 μm) and the cell (~5 μm) combined. HL-60 cells stably expressing GFP were used for TFM to track the outline of cells during the migration. Primary neutrophils were labeled with calcein AM (30 min, Invitrogen) or DiO (5 min, Invitrogen) and washed once with RPMI 1640 media prior to imaging studies. 532 (20 mW) and 635 (25 mW) nm diode-pumped solid state (DPSS) laser lines were used to excite the fluorophores within the cell and the beads. The exposure time for both channels was 21 msec. Using iXon EM+ DU-897 back illuminated EMCCD (Andor Technology), images of cells expressing GFP and fluorescent beads were captured interchangeably every 0.8 sec for each fluorescent channel during stimulation and after the cells completely detached from the substrate. Images of the beads were analyzed by a custom-made program to calculate bead displacement and to generate traction maps. Images of beads after cell detachment, therefore traction-free, were used as a reference.

For traction analysis, the leading edge of a polarized neutrophil was defined as the area within the first 3 μm of the cell (for control cells and cells treated with Y-27632), while the rest of the cell was defined as the trailing edge. For ML-7-treated, MLCK-depleted or blebbistatin-treated cells, the leading edge was defined as the area within the first 2.2 μm of the cell. These definitions were based upon quantifications of the leading-edge areas in HL-60 cells expressing the frontness markers such as YFP-actin and primary neutrophils stained with rhodamine-phalloidin for F-actin with or without the drug treatments or MLCK depletion. The average tractions at the leading and trailing edges were calculated from the traction maps generated by the use of TFM.

To determine the periodicity of the front and rear tractions, Fourier analysis was performed using the traction values obtained from the TFM. The analysis was done using the built-in MATLAB "fft" (Fast Fourier Transform) function to transform the original time-domain traction signals into frequency domain. The PSD plots were then generated based on the results from the Fourier transform analysis.

To analyze cross correlation between tractions at the leading and trailing edges and to calculate the cross-correlation coefficient (r) (Manders et al., 1992), a customized MATLAB (Mathworks) program was developed:

$$r = \frac{\sum_i \left(F_i - \overline{F}\right)\left(B_i - \overline{B}\right)}{\sqrt{\sum_i \left(F_i - \overline{F}\right)^2 \sum_i \left(B_i - \overline{B}\right)^2}},$$

where F_i and B_i are the mean traction values of the front and back at time point i, and $\overline{F}$ and $\overline{B}$ are the averaged mean traction values of the front and back over entire time. To examine the time lag between tractions at the leading and trailing edges, the values for tractions at the front were shifted in time with those at the back fixed.

Results

Tractions at both edges of chemotaxing neutrophils oscillate periodically with a time offset

To assess the spatial and temporal pattern of tractions in neutrophils during chemotaxis, we plated neutrophils on a flexible substrate coated with fibronectin and stimulated them with a point source of the chemoattractant formyl-Met-Leu-Phe (fMLP). Fibronectin has been widely used as a substrate for the study of neutrophil chemotaxis (Bain et al., 2003; Oakes et al., 2009; Wang et al., 2002). We used a substrate stiffness of 3.5 kPa, resembling the stiffness of tissue cells such as endothelial cells (1-5 kPa) (Janmey and McCulloch, 2007). We used both the neutrophil-like differentiated HL-60 (dHL-60) cells and human primary neutrophils. HL-60 cells, when differentiated, exhibit neutrophil-like morphologies, polarize and migrate in gradients (or in uniform concentrations) of attractants at rates comparable to those of neutrophils from peripheral blood, but unlike primary neutrophils they can be continuously cultured and are genetically tractable (Servant et al., 2000; Wang et al., 2002; Xu et al., 2003). Therefore,

HL-60 cells have been used widely as a model for studying neutrophil polarity and chemotaxis (Bodin and Welch, 2005; Gomez-Mouton et al., 2004; Hauert et al., 2002; Schymeinsky et al., 2006). We detected tractions at both the leading and the trailing edge of dHL-60 cells (Figure 2.1A). Tractions were not distributed evenly at the leading or the trailing edge but instead were often concentrated in small regions that ranged from 1 to 4 μm in diameter (Figure 2.1A; Supplementary Movie S1). Those "hot spots" of tractions varied in their lifetime, with some persisting for several seconds and others quite transient with a subsecond lifetime (data not shown). Most traction, especially around the cell periphery, was directed toward the cell center (data not shown).

Time-course analysis of tractions in cells moving towards fMLP revealed a highly dynamic temporal pattern: the mean level of tractions at both edges oscillated during migration (100-400 Pa) (Figure 2.1A-2.1B) (The average tractions are summarized in Table 2.1). Fast-Fourier transform (FFT) analysis of the time-domain signals revealed periodicity of tractions in chemotaxing neutrophils: the Power Spectral Density (PSD) plots of results from FFT analysis demonstrated a single pronounced peak at 4.8 ±1.4 sec for tractions at the leading edge and 4.8 ±1.6 sec for those at the trailing edge (means±SEM, n=9 cells) (Figure 2.1C). Primary human neutrophils showed a similar pattern of tractions. Tractions were detected at both edges, where they oscillated at a periodicity of 4.7±1.5 sec and 4.7 ± 1.0 sec, respectively (means±SEM, n=6 cells) (Fig. 2.1D). Interestingly, oscillations of tractions at the two edges were out of phase (Figure 2.1A), and the tractions at the front preceded those at the back by 0.80±0.23 sec [means±SEM (n=9 cells); $p<0.0001$] for dHL-60 cells and 0.40±0.16 sec [means±SEM (n=6 cells); $p<0.001$] for primary cells, as shown by a cross-correlation analysis, which computed the time offsets between tractions at the front and the back by shifting the two data sets relative to each other (Figure 2.1E and 2.1F). The conserved periodic and out-of-phase behavior of tractions at the neutrophil's front and back suggests a biomechanical mechanism that drives coordinated movements of neutrophils via differential contractile stresses exerted onto the substrate.

Figures and Tables

Figure 2.1

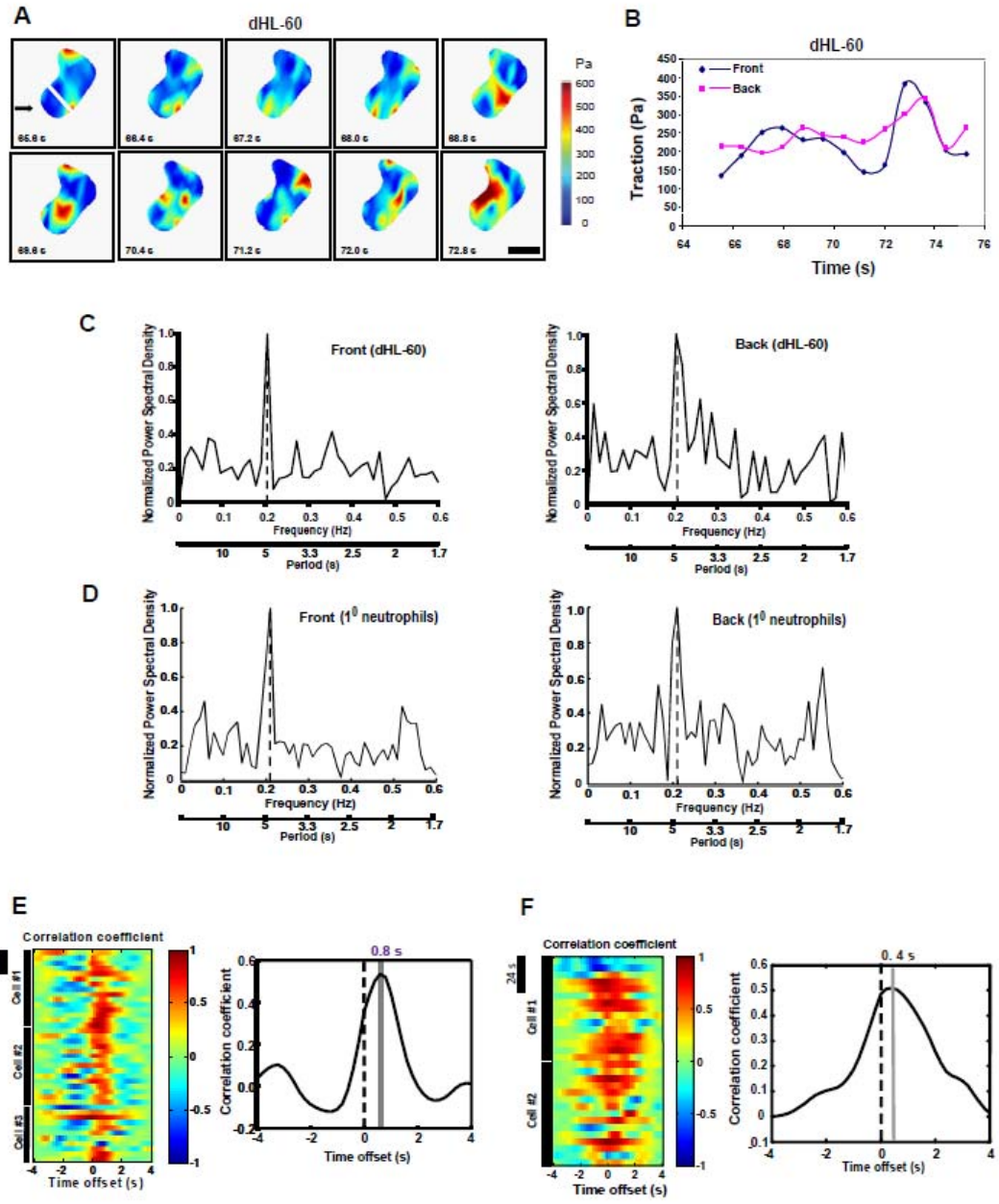

Figure 2.1 (cont.) Spatiotemporal dynamics of tractions during neutrophil chemotaxis

(A) dHL-60 cells were allowed to migrate toward chemoattractant-containing micropipette (fMLP, 10 μM) on a FN-coated elastic polyacrylamide gel for the times indicated. The speed for cell migration is approximately 2.0 μm/minute, lower than the speed of cells on FN-coated glass (2.4 μm/minute). The cells also exhibit normal tail retraction on the elastic gel (data not shown). Traction maps of the cell are shown. Pseudocolor bar representing tractions is given in Pascal (Pa). Scale bar represents 5 μm. Arrow indicates the direction of fMLP gradient. The leading edge of a polarized neutrophil was defined as the area within the first 3 μm of the cell (marked by a white line), whereas the rest of the cell was defined as the trailing edge ("Polyacrylamide gel substrates, TFM, and data analysis"). The image series shows part (~7.2 seconds, for which the cell traveled ~0.24 μm) of the whole migratory response. The video of the cell in panel A is available in supplemental data. (B) Time series of traction maps from panel A (with 3 additional time points) was analyzed by a customized MATLAB program to determine the average tractions in both leading edge (front) and trailing edge (back) of the cells in a time-dependent manner. The graph shows part (~9 seconds) of the whole migratory response. The x-axis indicates time in seconds; y-axis is in Pascal (Pa). The mean levels of tractions at the leading and the trailing edges were comparable. (C) PSD plots of tractions at the leading (left panel) and the trailing edge (right panel) of a migratory dHL-60 cell. PSD plots were generated based on the results from Fourier analysis of the traction values. The y-axis represents the power spectral density normalized to the highest peak value (~1); x-axis shows the oscillation frequency (Hertz; top) or period (seconds; bottom). Nine cells were analyzed, and a representative cell is shown. (D) PSD plots of tractions at the leading edge (left panel) and the trailing edge (right panel) of a migratory primary neutrophil. Six cells were analyzed, and data from a representative cell are shown. (E) Left panel: Cross-correlation between tractions at the leading edge and the trailing edge against time offset during migration for individual dHL-60 cells. Dotted lines indicate zero offset. Note that the back traction lags the front traction as indicated by the maximum cross-correlation at time offset of 0.8 seconds. Data from 3 representative cells are shown. Time bar represents 24 seconds. Right panel: Summary of time offsets between leading edges and trailing edges (n ~9 cells) in dHL-60 cells. (F) Left panel: Cross-correlation between tractions at the leading and the trailing edges against time offset during migration for individual primary neutrophils. Data from 2 representative cells are shown. Right panel: Summary of time offsets between leading edges and trailing edges (n=6 cells) in primary neutrophils.

	Front, Pa	Back, Pa
dHL-60 cells, 3.5 kPa		
Control	180 ± 39	207 ± 27
ML-7	111 ± 26	118 ± 30
MLCK KD	110 ± 16	145 ± 54
Blebbistatin	136 ± 19	112 ± 14
Y-27632	99 ± 16	87 ± 18
Primary neutrophils, 3.5 kPa		
Control	56 ± 17	85 ± 30
ML-7	40 ± 5	55 ± 7
Blebbistatin	33 ± 6	56 ± 11
Y-27632	33 ± 8	27 ± 3
Primary neutrophils, 100 kPa		
Control	596 ± 93	638 ± 102
ML-7	399 ± 87	375 ± 37
Blebbistatin	310 ± 88	390 ± 67
Y-27632	361 ± 83	349 ± 49

Table 2.1 Magnitude of tractions in migrating neutrophils
dHL-60 cells or primary neutrophils were allowed to migrate toward a chemoattractant-containing micropipette (fMLP, 10 μM) on a FN-coated elastic polyacrylamide gel for ~ 5 min. Prior to the chemotaxis assay, cells were treated with various pharmacological inhibitors (ML-7, Blebbistatin or Y-27632) or siRNA for MLCK. Polyacrylamide gels with two different stiffness, 3.5 and 100 kPa, were used in the assay. Average traction values at the leading and the trailing edges of the neutrophils undergoing chemotaxis under various conditions were measured and are summarized in the table.

CHAPTER 3

NONMUSCLE MYOSIN II REGULATES TRACTION AND MOTILITY IN NEUTROPHIL CHEMOTAXIS

Introduction

In this chapter, I address the role of nonmuscle myosin II in regulating traction and cell motility during neutrophil chemotaxis. Nonmuscle myosin II can induce contraction of the filamentous actin fibers. When such actin fibers are linked to the ECM through adhesion molecules, the pulling action of nonmuscle myosin II on actin can generate traction. Therefore we asked whether myosin II regulates traction in neutrophil chemotaxis. We found that nonmuscle myosin II is localized to both leading and trailing edges in polarized neutrophils. Myosin II is required for magnitude and periodicity of traction in neutrophils. In addition, myosin II activities are essential for smooth, persistent motility of neutrophils by promoting the stability of the leading edge and the contraction of the trailing edge. In particular, by comparing the differential effects of inhibiting Myosin II or ROCK – a myosin II kinase which is distinctly localized at the trailing edge and involved in contraction of the cell rear - on cell motility, we deduced that myosin II activities at the leading edge specifically function to promote stable protrusion of the leading edge.

Materials and methods

Reagents

Human fibrinogen and human serum albumin (low endotoxin) were from Sigma-Aldrich. Y-27632 was from Calbiochem. fMLP was from BioChemika. Human fibronectin was from BD Biosciences. Alexa fluor 488 phalloidin and rhodamine-phalloidin were from Molecular Probes. Rabbit anti-nonmuscle myosin II heavy chain A and B antibody were from Covance (Emeryville, CA).

DNA constructs

EGFP-tagged sMLCK construct was a gift from Anne Bresnick (Albert Einstein College of Medicine) (Poperechnaya et al., 2000). EGFP-tagged α5 integrin (Laukaitis et al., 2001) and mCherry-tagged myosin IIA (Vicente-Manzanares et al., 2007) were kindly provided by Rick Horwitz (University of Virginia). GFP-actin was from Clonetech. Information on PAK-PBD-YFP and PH-AKT-YFP was reported (Wang et al., 2002; Xu et al., 2003). GST-FN III_{9-11} was also described (Orr et al., 2006).

Western blotting

For western analysis, 1-2 million cells in modified HBSS buffer without serum were stimulated with or without 100 nM fMLP at RT. Stimulation was stopped by adding 2X Laemmli sample buffer with a cocktail of proteases and β-mercaptoethanol. Equal amounts of protein lysates were loaded on reducing SDS-PAGE gels. After electrophoresis, gels were immunoblotted with primary antibodies against proteins of interest, followed by appropriate secondary antibodies. Primary antibodies used included anti-antibody mouse anti-MLCK (1:1000), anti-nonmuscle myosin II heavy chain A (1:500), anti-nonmuscle myosin II heavy chain B (1:500), rabbit anti-Akt antibody (1:1000) and anti-phospho [Ser473]-Akt (1:200).

Immunostaining and confocal fluorescence microscopy and 3D reconstruction

For immunofluorescence in fixed cells, cells were stimulated with 1 μM fMLP in modified HBSS buffer (mHBSS) for the indicated time. Cells were extracted with 0.2% Triton X-100 for 10 min at room temperature (RT), fixed in 3.7% paraformaldehyde and immunostained. Antibodies were used at a dilutions of 1:200 (p-MRLC) and 1:500 (myosin heavy chain IIA) and immunostaining was performed as described (Wang et al., 2002). F-actin was assessed by incubating for 10 min at RT with 0.2 unit of Alexa Fluor 488 conjugated phalloidin. Immunostained cells were imaged using epifluorescence microscopy or confocal fluorescence microscopy.

Confocal optical sectioning was performed with an Andor Technology Revolution System Spinning Disk Confocal Microscopy system (Andor) coupled to an Olympus IX71 inverted microscope with Olympus 100x APO/1.4 NA objective. The refraction

index of immersion media was 1.515. Theoretical *xy*- and *z*-axes resolutions were 0.159 and 0.2 μm, respectively. Images were obtained using iXon EM+ DU-897 back illuminated EMCCD (Andor Technology). Confocal images were taken with 0.2 μm step size. Upon acquisition, the confocal images were deconvoluted with Autoquant X 2.1 software (Media Cybernetics, Inc., Silver Spring MD). The 3D structure of the actomyosin network was reconstructed from the deconvoluted images using IMARIS software (Bitplane).

Cell transfection and live cell imaging

For transient transfections, the AMAXA nucleofection system was used. Differentiated HL-60 cells (2 x 10^7, on day 5–6 after DMSO addition) were spun down and resuspended in nucleofector solution V. DNA (5 μg) or siRNA (3 μg) was added to the cells, and the cell-DNA mixture was subjected to nucleofection (program T-19). Nucleofected cells were transferred to 20 ml of complete medium. Subsequent assays were performed 3-6 h for the expression vectors and 24–48 h for siRNAs after transfection.

For live-cell imaging, cells were plated on human fibronectin-coated surface and stimulated either with a uniform concentration of 1 μM fMLP or a point source of 10 μM fMLP from a micropipette (internal diameter of 1 μm, pulled from a glass capillary), as described (Servant et al., 2000). Differential interference contrast (DIC) images, fluorescent images, and combined DIC/fluorescence images were collected with a Zeiss 40X NA 1.30 Fluar DIC objective or 63X NA 1.4 Plan Apochromat DIC objective on a Zeiss Axiovert 200M microscope. All images were collected with a cooled charge-coupled device camera (AxioCam MR3, Zeiss) and processed by ImageJ programs.

Lentivirus-mediated myosin IIA knockdown

The pKLO.1-puro lentiviral vectors containing scramble or myosin IIA-targeting shRNAs were purchased from Sigma. We used the Viralpower Lentivirus Packaging System (Invitrogen) to generate lentivirus according to the manufacturer's instructions. Briefly, HEK293T cells were plated and transfected on the second day with shRNA-containing plasmids using the Fugene 6 reagent (Roche). The medium was replaced the

next day with the virus packaging medium containing DMEM, 30% FBS, 1 mM sodium pyruvate, 4mM glutamine. Supernatant containing the lentivirus was collected 48-72 h later and was concentrated with ultracentrifugation (20,000 rpm, 1 h).

Concentrated viruses were added to differentiating HL-60 cells (on day 2) and incubated for 12 h. A multiplicity of infection (MOI) of 100 was used. Polybrene (6 μg/mL) (Sigma) was also added to the medium to improve the infection efficiency. Virus-containing medium was replaced with fresh culture medium, and cells were continuously cultivated for 4-5 d before subsequent analysis.

Results

Myosin II is localized at both edges of polarized neutrophils

Myosin II filaments can apply forces to move actin filaments relative to each other. During fibroblast migration, the contractile force generated by the actin-myosin cytoskeleton causes tractions on the underlying substrate by propagating through the actin-integrin-ECM link (Geiger and Bershadsky, 2002). We therefore assessed myosin II expression and spatial localization in neutrophils. Experiments with isoform-specific antibodies demonstrated that neutrophils mainly expressed myosin IIA (Figure 3.1A), consistent with an earlier report (Maupin et al., 1994). We then assessed the spatial localization of myosin II using antibodies against total myosin IIA, myosin regulatory light chain (MRLC) phosphorylated at Ser19 [p[19]-MRLC (Xu et al., 2003), the activated form of MRLC] and an mCherry-tagged myosin IIA (mCherry-myosin IIA) (Vicente-Manzanares et al., 2007) in fixed or live dHL-60 cells. Both total and activated myosin II and the mCherry-tagged fusion protein were located mostly at the trailing edge of polarized neutrophils (69%, 68% and 72% of total fluorescence intensity for myosin IIA, p[19]-MRLC and mCherry-myosin IIA, respectively) (Figure 3.1B and 3.1C; Supplementary Movies S2 and S3), consistent with earlier reports (Weiner et al., 2006; Xu et al., 2003). There was a considerable amount of myosin IIA localization at the front (31%, 32%, and 28%, respectively; Figure 3.1B and 3.1C), as described previously in studies on primary neutrophils (Bain et al., 2003; Pestonjamasp et al., 2006). Using confocal fluorescence microscopy combined with 3D reconstruction, we found that myosin IIA was enriched around the periphery of the uropod (trailing edge) and

distributed vertically and somewhat diffusely in the pseudopodia (Figure 3.1D; Supplementary Movies S4 and S5). Interestingly, although F-actin was highly enriched at the leading edge, it was also detected throughout the periphery of the cell including at the back of the cell (Figure 3.1D; Supplementary Movies S4 and S5).

Myosin II controls tractions and is required for neutrophil chemotaxis

We next impaired the function of myosin II in neutrophils and assessed the effect on tractions. As expected, inhibiting myosin II with blebbistatin (a specific myosin II inhibitor) in dHL-60 cells and primary neutrophils substantially reduced the tractions at both the leading and the trailing edge by up to 50% (Figure 3.2A and 3.2B) (Table 2.1). Remarkably, myosin II inhibition abolished the periodicity of tractions at both edges: myosin II-inhibited cells no longer exhibited periodic oscillations of tractions but instead showed random fluctuations, as shown by the lack of distinct frequencies/periods in all cells analyzed (n=10 for dHL-60 cells; n=6 for primary neutrophils) (Figure 3.2C and Figure 3.3A-B). Thus, myosin II is necessary for development and periodicity of tractions in neutrophils and serves as the molecular basis for tractions in neutrophils during chemotaxis.

Inhibition or depletion of myosin II also impaired neutrophil directional migration. In the presence of an fMLP gradient delivered by the micropipette, both dHL-60 cells and primary neutrophils, when plated on fibronectin-coated cover glass, polarized and rapidly migrated in the direction of the pipette with well-developed pseudopodia (Figure 3.4A and Figure 4.3A; Supplementary Movie S6). In contrast, cells treated with blebbistatin failed to persist in forward movement and formed poorly-developed, unstable, leading edges (Figure 3.4A; Supplementary Movie S7; data not shown). Differential interference contrast (DIC) kymographs of cells responding to the pipette stimulation demonstrated that blebbistatin-treated cells often retracted their leading edges after initial protrusion while untreated cells exhibited a persistent and progressive pattern of leading-edge protrusion (Figure 3.4B and Figure 3.5A-H). In addition, blebbistatin treatment caused defects in contractility at the back of the cells, which in many cases exhibited long, stretched tails (Figure 3.4A, Figure 3.5D and 3.5H), as previously reported (Xu et al., 2003). Differentiated HL-60 cells in which myosin IIA was depleted by small hairpin (sh)

RNAs exhibited similar (albeit less profound) defects (Figure 3.4A-B, Figure 3.5A-D and Figure 3.5I; Supplementary Movie S8). Thus, myosin II inhibition (or depletion) caused neutrophils to form unstable leading edges and long tails. In contrast, inhibition of p160-ROCK, a key component of the previously documented "backness" pathway that regulates neutrophil polarity and chemotaxis (Wong et al., 2006; Xu et al., 2003), reduced the level of activated myosin II at the back (Figure 4.7A), induced neutrophils to form long stretched tails (Figure 3.4A) (Alblas et al., 2001), but failed to affect protrusion of the leading edge (Figure 3.4A-B, and Figure 3.5A-H; Supplementary Movie S9). The backness pathway promotes localized activation of Rho and its downstream kinase p160-ROCK, leading to spatial activation of myosin II at the trailing edge (Wong et al., 2006; Xu et al., 2003). Based on the differential effects of myosin II and p160-ROCK inhibition on protrusion, we inferred that myosin II activity at the neutrophil's leading edge is necessary for stabilizing the protrusion response.

Figures

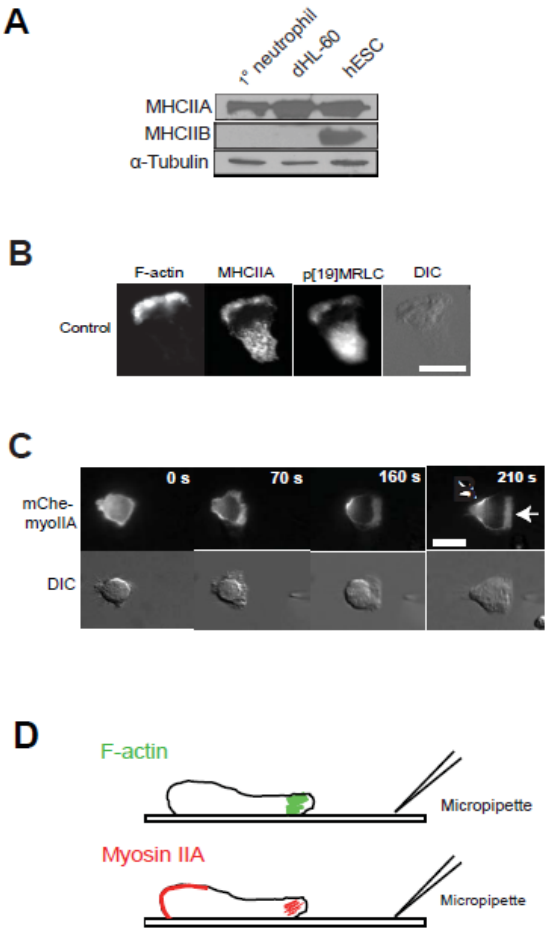

Figure 3.1 Expression and subcellular localization of nonmuscle myosin II in neutrophil chemotaxis

(A) Western blot analysis of primary human neutrophils and dHL-60 cells probed with mAbs specific for myosin II heavy chain isoform A (MHCIIA) and B (MHCIIB). Embryonic stem cells (human; denoted as hESC) expressed both myosin IIA and IIB and were used as a positive control. α-tubulin was used as a loading control. (B) dHL-60 cells were stimulated for 3 min by a uniform concentration of 1 μM fMLP. Cells were fixed with 3.7 % paraformaldehyde and stained with a specific anti-myosin heavy chain IIA (MHCIIA) antibody, anti-p[Ser19]MRLC antibody, and rhodamine-conjugated phalloidin to localize filamentous actin (F-actin). The corresponding DIC image is also shown. Bar, 10 μm. (C) dHL-60 cells were transfected with mCherry-myosin IIA (mChe-myoIIA) and

Figure 3.1 (cont.) stimulated by a micropipette containing 10 μM fMLP for the indicated times. mCherry-myosin IIA fluorescence and the corresponding DIC images are shown. Arrows point to the locations of myosin IIA at the leading and trailing edge. Bar, 10 μm. The movie of the cell in (C) is available in the Appendix. (D) Schematic view of myosin IIA localization in a polarized neutrophil after fMLP stimulation. The representation shows a cross-section of the neutrophil and is based on confocal fluorescence microscopy combined with 3D reconstruction. The movies showing 3D views of myosin IIA immunofluorescence are available (Supplementary Movies S4 and S5).

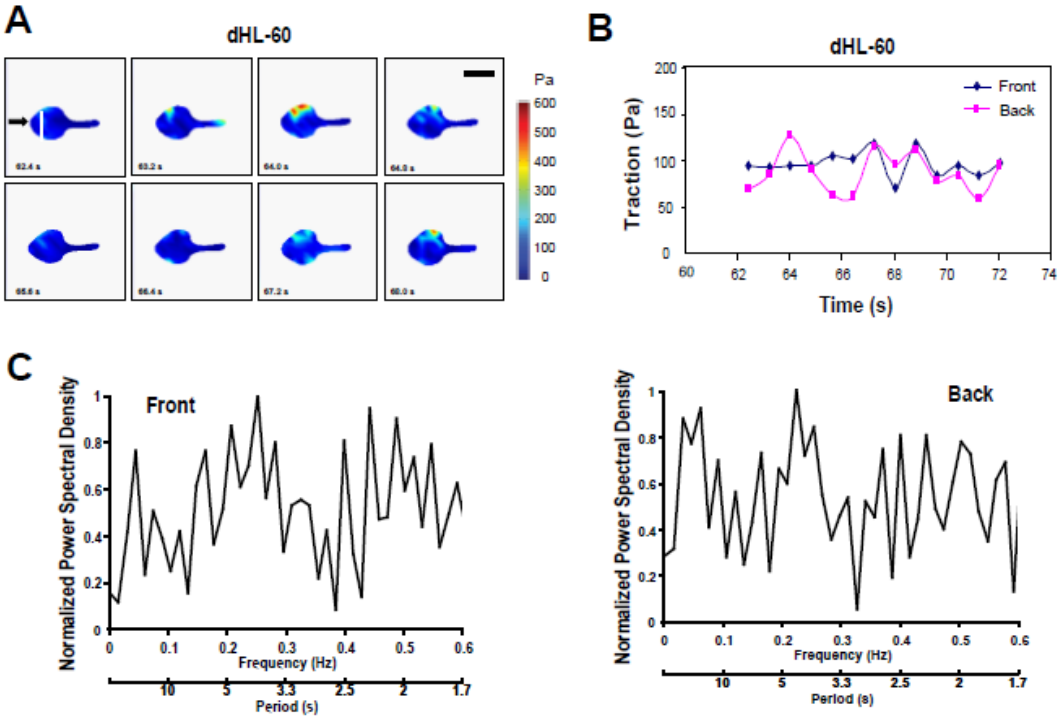

Figure 3.2 Myosin II controls tractions and is necessary for neutrophil chemotaxis
(A) dHL-60 cells pretreated with blebbistatin (100 μM, 30 min) were allowed to migrate toward chemoattractant-containing micropipette (fMLP, 10 μM) on a fibronectin-coated elastic polyacrylamide gel for the indicated times. Cells treated with blebbistatin migrated at 1.0 μm/min on the elastic gel. Traction maps of the cell are shown. Pseudocolor bar representing traction force is given in Pascal (Pa). Scale bar = 10 μm. The leading edge (within the first 2.2 μm of the cell) is marked by a white line (see Materials and Methods). The image series shows part (5.6 sec) of the whole migratory response. (B) Time series of traction maps from (A) (with four additional time points) was analyzed by a customized MATLAB program to determine the average tractions in both leading (front) and trailing edges (back) of the cells in a time-dependent manner. The graph shows part (~9.6 sec) of the whole migratory response. x axis indicates time in sec. y axis is in Pascal (Pa). (C) PSD plots of tractions at the leading (left panel) and the trailing edge (right panel) of a migratory cell pretreated with blebbistatin (100 μM, 30 min). The whole migratory response was analyzed. y axis represents the power spectral density normalized to the highest peak value (=1). x axis shows the oscillation frequency (Hz) (top) or period (s) (bottom). Cells depleted of myosin II exhibited similar response (not shown). 10 cells were analyzed, and a representative cell is shown. Additional plots are shown in Figure 3.3.

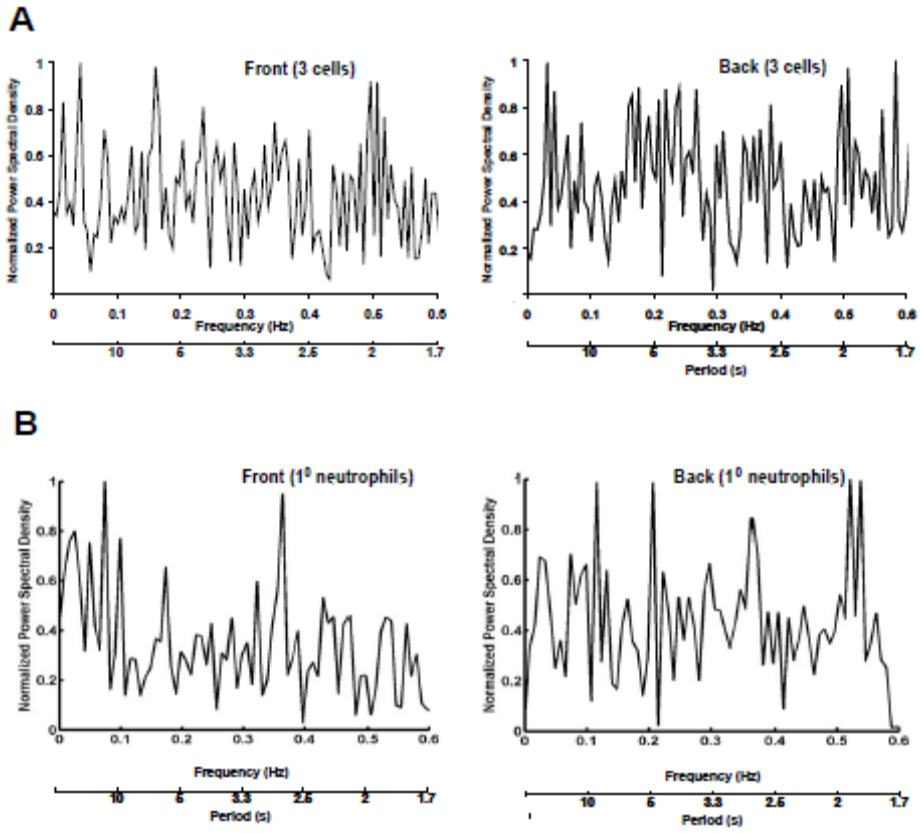

Figure 3.3 Myosin inhibition abolishes the periodicity of traction in neutrophils
(A) PSD plots of tractions at the leading (left panel) and the trailing edge (right panel) of three dHL-60 cells treated with blebbistatin (100 μM, 30 min). Tractions values from three cells were analyzed and combined in one plot. See Figure 2.1 legends for more details. (B) PSD plots of tractions at the leading (left panel) and the trailing edge (right panel) of a primary neutrophil treated with blebbistatin (100 μM, 30 min). 5 cells were analyzed, and a representative cell is shown.

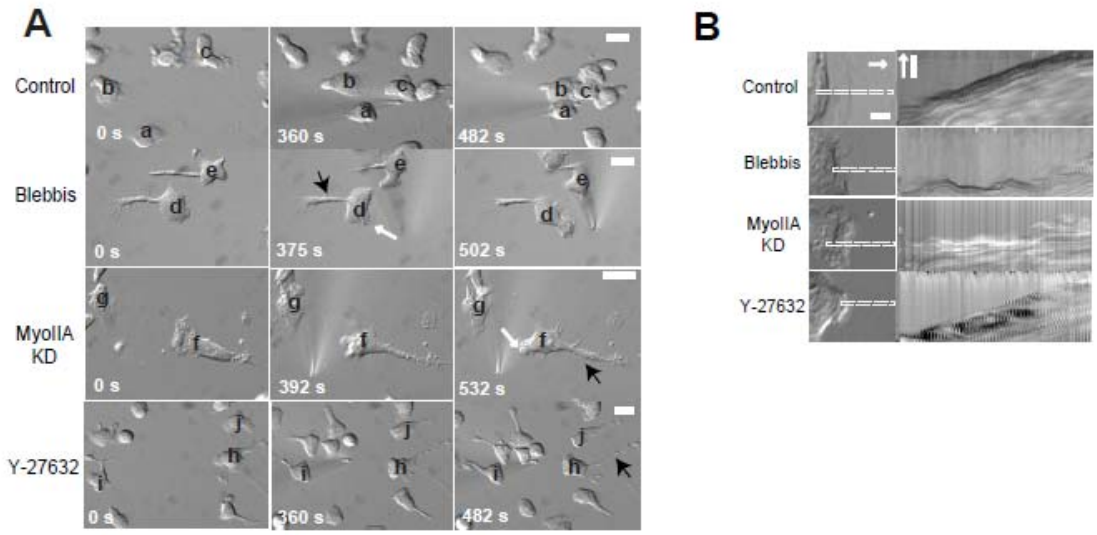

Figure 3.4 Myosin II activity at the leading edge is required for stable protrusion in neutrophil chemotaxis

(A) Before exposure to attractant supplied by a micropipette containing 10 μM fMLP, dHL-60 cells were not pretreated (control), were pretreated with blebbistatin (Blebbis, 100 μM, 30 min), were infected with lentivirus containing myosin IIA-targeting shRNAs (MyoII KD), or were pretreated with Y-27632 (30 μM, 30 min). The three images in each row show the positions of individual cells (each identified with a superimposed letter) after the indicated times of exposure to fMLP. White and black arrows point to the poorly-developed leading edges and long stretched tails, respectively. Cells infected with virus containing a scramble shRNA exhibited similar response to uninfected control cells. Lower doses of blebbistatin (≤50 μM) were tested, which required prolonged period of incubation to exert the same effects as 100 μM blebbistatin (data not shown). Scale bar, 10 μm. Movies of cells with or without treatments are available in the Appendix. (B) DIC kymographs of a dHL-60 cell untreated or treated with inhibitors or myosin IIA shRNAs migrating toward an fMLP (10 μM)-containing micropipette. The left panel shows a portion of the neutrophil's leading edge under various conditions. The dotted rectangles indicate the regions of the cell used to generate the kymographs (prior to fMLP stimulation). The actual lengths of the rectangles are 20 μm in the direction of the arrow. White scale bar =1 μm. The right panel shows the DIC kymographs. White scale bar=5 μm. In both panels white arrows indicate the direction of protrusion. Cells a, d, f and h in (B) were used for the analysis. ~8 min of migration was recorded.

Figure 3.5

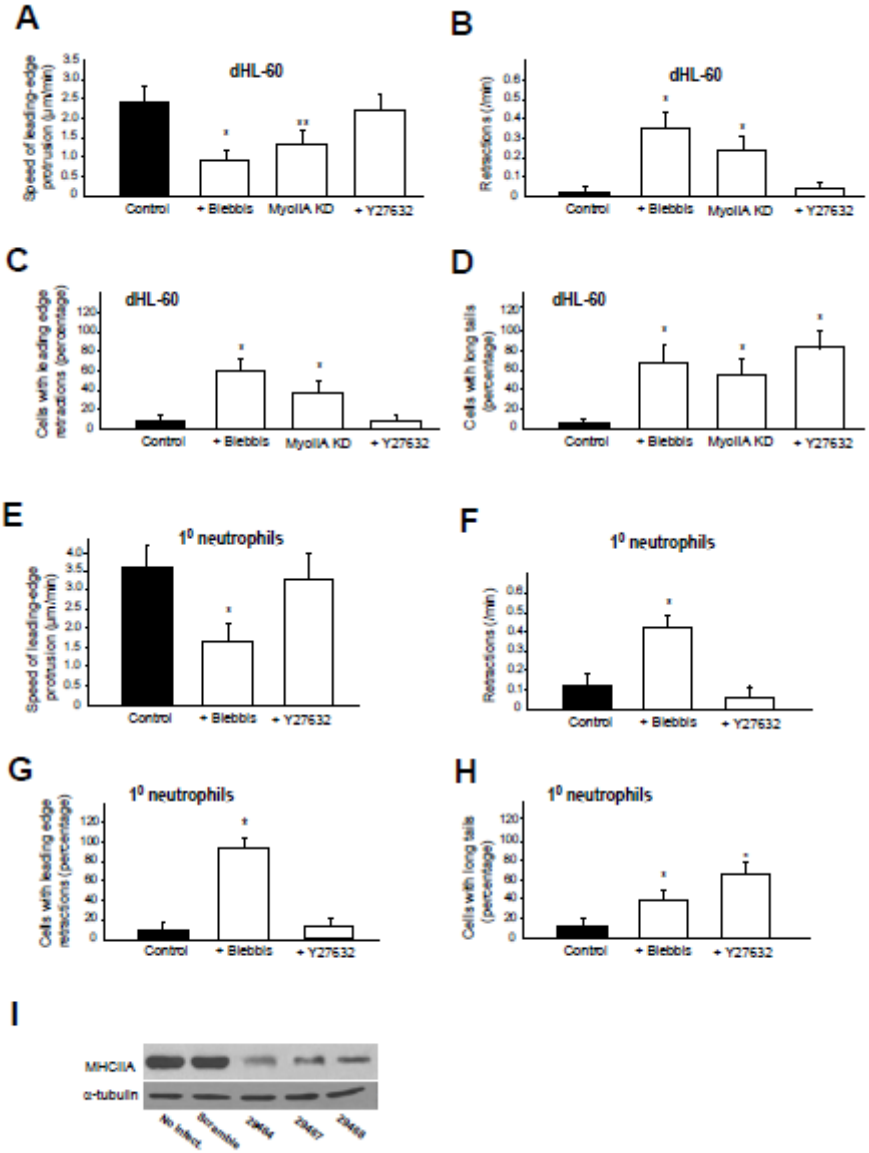
A
dHL-60
Speed of leading-edge protrusion (μm/min)
Control
+ Blebbis
MyoIIA KD
+ Y27632
B
dHL-60
Retractions (/min)
C
dHL-60
Cells with leading edge retractions (percentage)
D
dHL-60
Cells with long tails (percentage)
E
1⁰ neutrophils
F
1⁰ neutrophils
G
1⁰ neutrophils
H
1⁰ neutrophils
I
MHCIIA
α-tubulin
No infect.
Scramble
29464
29457
29459

Figure 3.5 (cont.) Myosin II activity at the leading edge is required for stable protrusion in neutrophil chemotaxis

(A and B) Speed of protrusion (A) and retraction frequency (B) of the leading edge in cells responding to a gradient of fMLP delivered by a micropipette. dHL-60 cells were not pretreated (control), pretreated with blebbistatin (Blebbis, 100 μM, 30 min), infected with lentivirus containing myosin IIA-targeting shRNAs (MyoII KD), or pretreated with Y-27632 (30 μM, 30 min). The value are means ± SEM (n = 27 for control, 26 for cells treated with Blebbistatin, 24 for myosin IIA-depleted cells, and 28 for cells treated cell Y-27632. Student t tests compared data between experimental groups. Results significantly different from those of control are indicated by asterisks (*, $p < 0.0001$; **; $p < 0.001$). (C and D) Percentage of dHL-60 cells demonstrating leading-edge retractions (C) and long stretched tails (D) when exposed to fMLP gradients. Cells retracting their leading edges at least once during migration were scored as positive. To define cells with long tails, we calculated ratios between the length and width in individual cells and used 2 as a cut-off value. Each bar represents the mean+SEM (error bars) of different numbers of cells that were tested in multiple experiments: 30 control cells and 27, 24, and 30 cells for Blebbistatin, myosin IIA depletion, and Y-27632, respectively. Asterisks indicate that the value for cells with the treatments differs from the corresponding control by $P < 0.0001$. (E-H) The same set of analysis for primary human neutrophils, which were not pretreated (control), pretreated with blebbistatin (Blebbis, 100 μM, 30 min), or pretreated with Y-27632 (30 μM, 30 min). The value are means ± SEM (n = 19 for control, 21 for cells treated with Blebbistatin, and 18 for cells treated cell Y-27632. Student t tests compared data between experimental groups. Results significantly different from those of control are indicated by asterisks (*, $p < 0.0001$). (I) Western blot of myosin IIA in dHL-60 cells with or without myosin IIA depletion. Infection of cells with viruses containing three separate myosin IIA-targeting sequences effectively depleted myosin IIA, when compared with cells without infection (no infect.) or cells infected with viruses containing a scramble shRNA or three myosin IIA-specific shRNAs. The shRNA sequence 29464 was used in Figure 3.4A. α-tubulin was a loading control. A typical experiment from four separate experiments is shown.

CHAPTER 4

MLCK-MEDIATED ACTOMYOSIN CONTRACTILITY IS REQUIRED FOR TRACTION AND PROMOTES LEADING EDGE STABILITY BY REGULATING α5β1-INTEGRIN ACTIVATION

Introduction

In this chapter, I address the role of myosin light chain kinase (MLCK) in controlling myosin II activities, traction and integrin activities in neutrophil chemotaxis. MLCK is known to be involved in myosin II activation in other motile cells. Therefore, we asked whether MLCK regulates myosin II in neutrophils. We found that MLCK is recruited selectively to the leading edge upon chemoattractant-mediated activation of neutrophils and activates myosin II at the leading edge. Such MLCK-mediated actomyosin contractility is important for generating periodic traction pattern in neutrophils. Furthermore, MLCK-driven contractile force allows stable protrusion of the leading edge by regulating α5β1-integrin activation.

Materials and methods

Reagents

ML-7 was from Sigma-Aldrich. Human recombinant ICAM-1 was from R&D Systems. ON-TARGETplus SMARTpool siRNAs containing four siRNAs specifically targeting human MLCK, non-specific siRNAs and siGLO were from Dharmacon. The GRADSP and GRGDSP peptides were from Biomol. Mouse or rabbit anti-MLCK antibodies were from Sigma-Aldrich or generated as described (Wilson et al., 1991). Mouse anti-GST antibody was from Santa Cruz Biotechnology. Rabbit anti-phospho [Ser19] myosin light chain antibody, rabbit anti-Akt antibody, and rabbit anti-phospho [Ser473]-Akt antibody were from Cell Signaling Technology.

Adhesion assay

Neutrophil adhesion to 96-well tissue culture plate was evaluated as described by Ryu *et al.* (Ryu et al., 2000). After stimulation by chemoattractant, cells pretreated with

or without ML-7 were allowed to adhere to a 96 well-plate, which was coated with fibronectin (100 μg/ml) and blocked with 2% BSA in PBS, at 37°C for 30 min. Non-adherent cells were removed by washing, and adherent cells were fixed with 3.7% PFA and stained with crystal violet (0.1% in 10% methanol). Stained cells were thoroughly washed and lysed with 1% SDS, and the absorbance from each sample was measured at 590 nm by a microplate reader (SpectraMax M2).

Micropipette assay in suspension

The procedure was modified from a previous report (Zhelev et al., 2004). Micropipettes for holding a cell and applying chemoattractant were mounted on the microscope stage. Eppendorf's programmable micromanipulator, the TransferMan NK 2, was used in the holding (left) side, while Injectman NI 2 was used for application of chemoattractant (right side). A single, round non-stimulated neutrophil was held in a holding pipette with an internal diameter of 5 μm (World Precision Instruments). Another pipette with an internal diameter of 1 μm was filled with 10 μM fMLP and positioned 5 μm from the cell surface. Suspended cells were gently held with CellTram Air connected to TransferMan NK 2 while precise delivery of chemoattractants was carried out from the right side with CellTram Vario. Chemoattractant-containing solution was blown over the cell, which initiated the extension of a single pseudopod. Pseudopod extension was observed in an inverted microscope (Leica DM IRE2) with a 40X objective. Images were captured with a charge-coupled device camera (Hamamatsu, C4742-95-12ERG) and analyzed with ImageJ software. The rate of pseudopod extension was calculated from the measured pseudopod lengths in time lapses.

Rac activation assay

To determine Rac-GTP levels in dHL-60 lysate, we used an absorbance-based (490 nm) Rac G-LISA kit (Cytoskeleton, Inc). dHL-60 cells were preincubated for 30 min with ML-7 (25 μM), centrifuged for 5 min at 2,000 rpm at RT, resuspended in mHBSS (2×10^6 cells in 0.5 ml per condition), and stimulated or unstimulated with 100

nM fMLP. The reaction was stopped by adding 0.5 ml of 2× lysis buffer (provided with the kit) at 4°C. Subsequent steps were performed as described in the protocol attached to the kit.

Measurement of polymerized actin

The procedure for measuring polymerized actin has already been described (Fumagalli et al., 2007; Weiner et al., 2006). Briefly, cells (pretreated with or without ML-7, 30 min) were stimulated in mHBSS in suspension with 1 μM fMLP at RT. After fixation by 2% paraformaldehyde for 20 min at 4°C, cells were permeabilized with 0.2% Triton X-100 and stained with 0.2 μM rhodamine-phalloidin for 30 min on ice. Stained cells were resuspended in ice-cold PBS, and fluorescence was determined by flow cytometry with a BD Biosciences LSR II System. The mean fluorescence intensity of the cell population was determined.

TIRF microscopy

For TIRF microscopy, a TIRF module based on Axiovert 200M microscope (Zeiss) was used as a starting point. Before each experiment, 488-nm excitation light from a 100-mW multiline argon-ion laser (Zeiss) was aligned properly to create evanescent wave that can only excite the molecules within a layer of 100 nm above the cover glass. At the start of an experiment, a fibronectin-coated cover glass to which fluorescing cells were attached was placed on top of α Plan-Fluar 100x /1.45 oil objective lens. Microscopic images from the TIRF-illuminated cells were captured by AxioCam MR3 camera with an interval of 5 sec for indicated time. Exposure times for each image were typically less than 1 sec, and the TIRF laser was shuttered with a Uniblitz COM2 shutter between exposures to minimize photodamage and photobleaching effects.

Integrin activation assay

A GST-tagged protein composed of 9th, 10th, and 11th fibronectin (FN) type III repeats (denoted as GST-FN III_{9-11}) was used to monitor active α5β1 integrin as reported (Orr et al., 2006). The GST-FN fragment binds to unoccupied active integrins only. For adherent cells, integrin activation was determined as follows. After exposure to

chemoattractant or buffer, cells were fixed with paraformaldehyde (3.7%) and incubated with 50 μg/ml GST-FN III_{9-11} in PBS with 1 mM Ca^{2+}/1 mM Mg^{2+} at 37°C for 30 min. Because the GST-FN fragment competes with the FN substrate to some extent, fixation of cells could eliminate interference from the FN substrate. After incubation with GST-FN III_{9-11}, Cells were gently washed, lysed in SDS sample buffer, and bound GST-FN III_{9-11} was blotted with an anti-GST antibody (1:1000). For immunofluorescence studies, after fixation, cells were incubated with GST-FN III_{9-11}, followed by Alexa-conjugated secondary antibody. For suspended cells, a similar procedure was used, except that the cells were not fixed. A rabbit anti-α5 integrin antibody (1:1000) was used to assess the total level and localization of α5 integrin.

Results

MLCK is expressed and recruited to the leading edge in chemotaxing human neutrophils

We next explored how localization-specific myosin II activity and tractions were controlled at the leading and the trailing edge. Earlier studies demonstrated that the spatial activation of myosin II at the trailing edge is dependent on p160-ROCK and necessary for tail retraction and de-adhesion (Wong et al., 2006; Xu et al., 2003). We thus sought to understand how myosin II was spatially activated at the leading edge in neutrophils. MLCK, a [Ca^{2+}]/calmodulin-dependent kinase, phosphorylates MRLC and induces contractility in multiple processes (Kamm and Stull, 2001), including cell motility (Klemke et al., 1997; Wilson et al., 1991). To ask whether MLCK spatially regulated myosin II activation at the leading edge of neutrophils, we first examined its expression and subcellular localization.

We examined the expression of MLCK in neutrophils. Western blotting indicated that both primary blood neutrophils and dHL-60 cells mainly expressed the ~130-kD short form of MLCK (Figure 4.1A); the 210-kD long form was nearly undetectable. This pattern was similar to that in human T lymphocytes (Smith et al., 2003), suggesting that predominance of the short MLCK form may be common to leukocytes.

In non-stimulated neutrophils, MLCK was diffusely distributed in the cytosol, with some cortical localization (Figure 4.1B). When stimulated with fMLP, it was recruited to the leading edge of polarized cells and co-localized with F-actin (Figure

4.1B). The polarized recruitment was confirmed by ectopic expression of EGFP-tagged short form MLCK (sMLCK-EGFP) (in accordance with its expression in neutrophils). Upon uniform fMLP stimulation of dHL-60 cells, sMLCK-EGFP translocated from the cytosol to the plasma membrane within 30–45 sec (Figure 4.1C; Supplementary Movies S10 and S11). As cells polarized morphologically, typically by 2–3 min, sMLCK-EGFP was recruited to the leading edge. The asymmetric recruitment of MLCK was also seen in neutrophils polarizing and moving toward a point source of fMLP delivered by micropipette (Figure 4.1D). Furthermore, MLCK asymmetry was not caused by increased amounts of membrane in ruffles at the front, because the GFP-tagged N-terminal fragment of protein Lyn (24 amino acids; Lyn24-GFP) (Gupta and DeFranco, 2003), which associates with the plasma membranes via myristoylation and palmitoylation, was distributed uniformly around the plasma membranes (Figure 4.1E). The recruitment of MLCK to the leading edge is dependent upon actin binding via actin binding domain (ABD) near the N terminus of MLCK, as selective deletion of ABD in MLCK prevents translocation of the mutant MLCK molecule to the leading edge (data not shown).

MLCK is required for the stable protrusion of the leading edge

MLCK inhibition by a highly specific inhibitor ML-7 (25 μM) impaired the stability of the leading edge and markedly reduced the speed of protrusion of dHL-60 cells and primary neutrophils, as shown by experiments with the micropipette assay (Figure 4.2 and 4.3). Similar to myosin II inhibition, MLCK inhibition caused neutrophils to often retract their leading edges during migration (~ 0.4/min and 0.03/min for treated and untreated dHL-60 cells, respectively; ~ 0.7/min and 0.15/min for treated and untreated primary cells, respectively). However, unlike myosin II inhibition, MLCK inhibition failed to induce formation of stretched tails at the back of the cells (Fig. 4.2B and Fig. 4.3A).

In circulating neutrophils β2-integrins are highly expressed and mediate the interactions with the endothelial cells. We thus assessed whether MLCK was also required for chemotaxis of neutrophils stimulated on ECM substrates for β2-integrins. Differentiated HL-60 cells, when stimulated by a fMLP gradient on fibrinogen or Inter-Cellular Adhesion Molecule 1 (ICAM-1) (Figure 4.4 and data not shown), rapidly

polarized and migrated towards the source of the chemoatractants ((Figure 4.4). ML-7 treatment markedly impaired the leading edge stability of these cells (Figure 4.4). These results suggest that MLCK might play a conserved role in the regulation of neutrophil polarity and chemotaxis under different microenvironmental settings.

The specificity of ML-7 for MLCK, instead of for other protein kinase including protein kinase A (PKA), was demonstrated at a similar concentration (Bain et al., 2003). Nevertheless to further confirm the specificity of MLCK, we used RNAi-mediated MLCK knockdown to deplete MLCK in dHL-60 cells. The Amaxa Necleofection System allowed us to deliver siRNAs into nearly all the cells after transfected and was used to transiently express siRNAs that selectively target MLCK (Figure 4.5A and 4.5B). The efficacy of the siRNAs to deplete MLCK was confirmed by assessing the level of endogenous MLCK, in the presence of either non-targeting siRNAs or siRNAs against MLCK (Figure 4.5A). MLCK depletion induced dHL-60 cells to exhibit defects in protrusion and migration similar to those caused by ML-7, whereas the non-targeting siRNAs exerted no effects (Figure 4.5C-4.5D).

Notably, the migratory defects in cells treated with ML-7 or with MLCK depleted were more severe than mouse neutrophils deficient in MYLK, the 210 kD isoform of MLCK (Xu et al., 2008). When plated on fibrinogen and exposed to chemoattractants, the MYLK-deficient mouse neutrophils polarized normally, migrated faster than the wild-type cells, but frequently changed direction. A possible explanation for the discrepancy is that ML-7 or siRNAs targets both isoforms of MLCK in dHL-60 cells while only the 210 kD form is deleted in MYLK-deficient mouse neutrophils (Xu et al., 2008).

We previously showed that the leading-edge activity is mediated by the frontness signaling pathway (Srinivasan et al., 2003; Wang et al., 2002; Xu et al., 2003). To provide a mechanistic explanation for the defects caused by MLCK inhibition and depletion, we assessed the effect of MLCK inhibition on frontness signals by monitoring the behavior of PH-AKT-GFP (GFP-tagged PH domain of the protein kinase Akt/PKB, readout for PI3Ps (Servant et al., 2000), PAK-PBD-YFP (yellow fluorescence protein-tagged p21-binding domain of PAK, readout for Rac-GTP in dHL-60 cells (Srinivasan et al., 2003), and actin-YFP in living cells with or without MLCK inhibition. As described earlier, an fMLP gradient delivered by a micropipette induced cells to polarize and

migrate persistently towards the tip of the micropipette (Figure 4.6A, left panels). Upon fMLP stimulation, these fluorescent probes translocated from cytosol and accumulated at the leading edge of chemotaxing cells. The recruitment of PI3Ps, Rac-GTP and polymerized actin in pseudopods was robust and stable, as indicated by both the loss of cytosolic GFP (or YFP) signals after stimulation and their strong asymmetric localization at the neutrophil's leading edge during migration. A quantitative analysis of the asymmetry in fluorescence intensity across the cells revealed a steep gradient of the fluorescent signal in untreated control cells (61, 85, and 67% decrease for PH-AKT-GFP, PAK-PBD-YFP and actin-YFP over a distance of 10 μm, respectively) (Figure 4.6B). In contrast, ML-7 treated cells under the same conditions exhibited poor leading edge recruitment of PH-AKT-GFP, PAK-PBD-YFP and actin-YFP, as reflected by much smaller gradients (21, 36, and 11%, respectively) (Figure 4.6A and 4.6B). Moreover, when compared with control cells, ML-7-treated cells exhibited a marked reduction (30–50%) in the ratio of mean fluorescence intensity between the leading edge and cytosol (i.e., mean intensity at front/mean intensity at the back), again revealing an impaired asymmetric recruitment of the frontness markers (Figure 4.6C). The use of ratio of mean fluorescence intensity discounts the variations in the levels of fluorescence probes among cells and is thus more appropriate for assessing the relative accumulation of the fluorescent signals at the leading edge. Similar to ML-7 treatment, MLCK depletion also impaired the recruitment of the frontness markers (Figure 4.5E).

To summarize, consistent with their effects on the leading edges, MLCK inhibition and depletion prevented accumulation of polymerized actin, 3'-phosphoinositol lipids (PI3Ps) and Rac-GTP at the leading edge. Actin polymers, PI3Ps and Rac-GTP are key components of the "frontness" pathway and play essential roles in establishing the leading edge during neutrophil chemotaxis (Srinivasan et al., 2003; Xu et al., 2003). Thus, our results show that MLCK is spatially recruited to the leading edge and is necessary for leading edge stability during neutrophil chemotaxis.

MLCK regulates myosin activity at the leading edge

MRLCs are the only known substrate for MLCK (Kamm and Stull, 2001). The asymmetric distribution of MLCK prompted us to ask whether this kinase would

selectively control the activity of myosin II at the leading edge. The ratio of mean immunofluorescence intensity of p[19]-MRLC between the leading and the trailing edge was ~25% lower in ML-7-treated dHL-60 cells than in the control cells (Figure 4.7A and 4.7B), suggesting that MLCK inhibition impaired the accumulation of activated myosin II at the leading edge compared with the rest of the cell body. The use of ratio of mean fluorescence intensity discounts the variations in the levels of fluorescence probes among cells and is thus more appropriate for assessing the relative accumulation of the fluorescent signals. Furthermore, treatment with the p160-ROCK inhibitor Y-27632 sharply reduced the distribution of phosphorylated myosin II at the trailing edge (Figure 4.7A), in keeping with an earlier report (Xu et al., 2003). Inhibition of myosin II activity by ML-7 and Y-27632 was also demonstrated by western blotting of total p[19]-MRLC levels (Figure 4.7C). Intriguingly, both ML-7 and Y-27632 treatments increased the relative distribution of myosin IIA protein at the leading edge (Figure 4.7D; 24% and 41%, respectively), probably due to the alterations in cytoskeletal organization. Taking into account the increased distribution of myosin IIA at the front, we inferred that ML-7 caused >30% decrease in the relative level of activated myosin II (i.e., p[19]-MRLC/total myosin IIA) at the leading edge.

MLCK-mediated actomyosin contractility regulates traction in neutrophil chemotaxis

Inhibiting or depleting MLCK in neutrophils markedly reduced the tractions at the leading edge (Figure 4.8A and 4.8B; Supplementary Movie S12) in cells migrating on the substrate with 3.5 kPa of stiffness (Table 2.1). Interestingly, the same treatments also reduced the tractions at the trailing edge (Figure 4.8A and 4.8B) (Table 2.1). Furthermore, MLCK inhibition (or depletion) abolished the periodic pattern of tractions at both the leading and the trailing edge in dHL-60 cells and primary neutrophils (Figure 4.8B-C, Figure 4.9A-B and Figure 4.10A). Because the tractions in MLCK-inhibited/depleted cells were reduced at both edges and were no longer periodic. This finding suggested coordination and coupling of tractions at the front and the back under this matrix stiffness. In keeping with this notion, treatment of cells with Y-27632 also substantially reduced the tractions and prevented the periodic oscillations at both the leading and the trailing edge (Figure 4D-4F, Figure 4.9C and Figure 4.10B) (Table 2.1).

It was recently documented that the chemotactic behaviors of neutrophils were influenced by substrate stiffness (Oakes et al., 2009). To investigate whether MLCK played a more conserved role in the regulation of tractions, we assessed the effect of MLCK inhibition in neutrophils migrating on a stiffer substrate (100 kPa). Primary neutrophils migrating towards a fMLP-containing micropipette exerted higher tractions under this condition, in keeping with the previous report (Oakes et al., 2009) (Table 2.1). Tractions at the leading and the trailing edge both demonstrated periodicity (4.7 ±1.5 sec and 4.7 ±1.0 sec, respectively) and were out of phase by 1.0±0.3 sec (Figure 4.11A and 4.11B). Myosin II inhibition, as expected, markedly reduced the levels and prevented the periodicity of traction at both edges (Figure 4.12A). MLCK inhibition exerted very similar effects on tractions to blebbistatin treatment (Fig. 4.12B). Intriguingly, although treatment of cells with Y-27632 reduced tractions by 40-45% (Table 2.1), the cells nevertheless exhibited periodic tractions at both edges (4.7±0.9 sec and 5.0±1.3 sec, respectively) (Figure 4.11C), with a lag of 0.90 ± 0.33 sec (Figure 4.11D). These results suggest a differential regulatory pattern of tractions in cells migrating on the stiffer substrate.

MLCK-driven contractile force controls leading edge adhesion by activating α5β1-integrin

How does MLCK-mediated myosin contractility control leading-edge stability in neutrophils? During migration protrusion and adhesion of the leading edge are tightly coupled (Ridley et al., 2003). Cell adhesion sites are required to stabilize leading edges and promote cell polarity in cells migrating on flat surfaces (Ridley et al., 2003). MLCK-mediated myosin II contractility may be necessary for leading edge protrusion. Alternatively, the defects of MLCK inhibition (or depletion) on neutrophil polarity can be interpreted as the inability of the cells to attach their protrusive pseudopods, resulting in unstable and poorly developed leading edges. Indeed, blocking leading edge adhesion of neutrophils with RGD peptides targeting α5β1–integrin, the main fibronectin receptors in neutrophils, caused defects highly reminiscent of those induced by MLCK inhibition, as discussed in detail below.

MLCK-inhibited fibroblasts exhibit defects in assembly (Totsukawa et al., 2004b) or turnover (Webb et al., 2004) of focal adhesions. Cell adhesion sites are required to stabilize leading edges and promote cell polarity (Ridley et al., 2003). To assess the role of adhesion in regulating neutrophil polarity during chemotaxis, we plated dHL-60 cells on fibronectin and then treated them with a soluble RGD peptide that inhibits binding of α5β1-integrin to fibronectin (α5β1-integrins are the main fibronectin receptors in neutrophils (Staffan Johansson, 1997)) before fMLP stimulation. This procedure allowed us to selectively prevent fMLP-induced de novo adhesion. An RAD peptide was used as a negative control. With a point source of fMLP in the presence of RAD peptide, dHL-60 cells migrated to the pipet tip and maintained a highly polarized morphology with well-developed pseudopods (Figure 4.13A and 4.13B). In contrast, cells treated with the RGD peptide only transiently polarized in response to fMLP, with much smaller and less stable leading edges that often retracted after protrusion, resulting in a less polarized, slowly migrating cell (Figure 4.13A-C). Thus, blocking cell adhesion caused defects that mirrored those caused by MLCK inhibition (Figure 4.2B).

MLCK inhibition markedly impaired neutrophil adhesion. First, experiments with a commonly used cell plating assay demonstrated that MLCK inhibition compromised adhesion of dHL-60 cells to fibronectin (Figure 4.14A). Interestingly, MLCK inhibition specifically prevented cell adhesion induced by fMLP, because ML-7 had little effect on cell adhesion to fibronectin in the absence of fMLP stimulation (Figure 4.14A). To further analyze adhesion at the single cell level, we used total internal reflection fluorescence (TIRF) microscopy in dHL-60 cells expressing GFP-tagged α5–integrin. The goal of this experiment was to assess whether MLCK inhibition impaired α5β1–integrin-mediated leading edge attachment. The evanescent wave causes excitation of fluorescent molecules in an optical section (<100 nm) without exciting molecules throughout the specimen and allows visualization of signaling activity in living cells in contact with the coverglass (substrate). TIRF microscopy analysis suggested that in response to a point source of fMLP gradient, neutrophils extended a protrusive leading edge and established contact with the fibronectin substrate, as indicated by the emergence of GFP fluorescence at the leading edge (Figure 4.14C). In addition, de-adhesion and retraction of trailing edge was apparent, as suggested by the disappearance of GFP

fluorescence at the trailing edge of migrating cells (Figure 4.14C). MLCK inhibition markedly impaired leading edge attachment, as suggested by the absence or reduction of fluorescent signals of GFP-α5 integrin at the leading edge (Figure 4.14D). We analyzed attachment quantitatively in control and MLCK-inhibited cells by measuring TIRF signals within the leading edge (as defined by DIC images) (Figure 4.14B). This analysis suggested that MLCK inhibition reduced leading edge adhesion by 78% (Figure 4.14B). In contrast, the same treatment only slightly altered attachment of the area outside the leading edge (denoted as Cell body) (Figure 4.14B: right panel). Thus, MLCK inhibition impaired leading edge adhesion. However, these results alone could not distinguish whether MLCK mediates leading edge protrusion or adhesion, as discussed above. As expected, cells treated with Y-27632 exhibited long stretched tail that failed to retract properly, while cells with blebbistatin treatment showed defects in both leading edge attachment and tail retraction (Figure 4.14E-F).

We next asked whether MLCK was necessary for leading edge protrusion. We took advantage of a feature of neutrophils: their ability to polarize when stimulated with chemoattractants, even in suspension. When exposed to fMLP, neutrophils in suspension quickly (within 1–2 min) establish a morphological leading edge (Zhelev et al., 2004). The leading edge does not persist and retracts after stimulation (Fechheimer and Zigmond, 1983; Sklar et al., 1985; Wang et al., 2002; Ydrenius et al., 1997). Attractant stimulation of neutrophils in suspension also suffices to lead to accumulation of polymerized actin, PI3Ps and Rac-GTP, albeit transiently, consistent with the morphological response (Srinivasan et al., 2003; Wang et al., 2002; Xu et al., 2003). When held with a pipette, dHL-60 cells responded to a gradient of fMLP from an adjacent pipette by extending a leading edge (Figure 4.15A). The leading edge continued to grow and then retracted. Cells treated with ML-7 exhibited no detectable defects in the protrusive behavior and dynamics when stimulated with the fMLP gradient (Figure 4.15A and 4.15B). We next measured the level of polymerized actin, Rac-GTP and phospho-Akt (activated Akt, readout for PI3Ps) (Wang et al., 2002; Xu et al., 2003) with or without fMLP stimulation. Consistent with previous findings (Srinivasan et al., 2003; Wang et al., 2002; Xu et al., 2003), fMLP addition induced a rapid and transient accumulation of polymerized actin, phospho-Akt and Rac-GTP in neutrophils in suspension, which peaked at 30─60 sec after

stimulation (Figure 4.15C-E). Treatment with ML-7 failed to prevent any of these frontness markers in cells exposed to fMLP in suspension (Figure 4.15C-E). Therefore, MLCK is not required for protrusion per se but appears to regulate leading edge adhesion. In addition, because MLCK inhibition/depletion impaired the leading-edge accumulation of PI3Ps, Rac-GTP and actin polymers in adherent cells (Figure 4.5E and 4.6), these results imply that cell adhesion is necessary for the stability of the frontness signals.

Integrin activation refers to a switch from a low-affinity to a high-affinity state of ligand binding. Integrin activation is the key step for cell adhesion to the ECM (Hynes, 2002). To explain how MLCK controls cell adhesion during neutrophil chemotaxis, we tested if MLCK is involved in integrin activation during chemotaxis. We assessed the localization and expression of activated α5β1-integrin with a GST-tagged protein containing the 9^{th} to 11^{th} fibronectin type III repeats (GST–FN III_{9-11}), which specifically binds active α5β1-integrin (Orr et al., 2006). While total α5β1-integrin (as detected by anti-α5-integrin antibody) was found evenly distributed throughout the cell, activated α5β1 integrin was enriched at the leading edge of polarized dHL-60 cells [Figure 4.16A; A focal plane from the confocal microscopy analysis is shown]. Consistently, the line profile of the polarized cell exhibited highest level of GST–FN III9-11 binding at the leading edge (Figure 4.16A). MLCK inhibition caused the level of active α5β1-integrin to markedly reduce at the leading edge, whereas the localization pattern of total α5β1-integrin remained unchanged (Figure 4.16B). Incubation of cells with GST alone failed to produce fluorescent signals (Figure 4.16C). These results suggest that MLCK controls α5β1-integrin activity at the neutrophil's leading edge.

We next assessed the level of activated α5β1-integrin in cells with or without MLCK inhibition biochemically. As shown in Figure 4.16D, ML-7 exerted little effect on fMLP-induced activation in neutrophils in suspension, indicating that MLCK activity is not necessary for the inside-out activation of α5β1-integrin by fMLP (i.e., in the absence of adhesion to ECM). However, the same treatment prevented α5β1-integrin activation when cells were attached to the fibronectin substrate (Figure 4.16E), demonstrating that MLCK is necessary for α5β1-integrin activation in adherent cells. The dependence of MLCK-mediated integrin activity on cell-ECM adhesion suggested that tractions may

play a special role in this regulation. Traction-induced cytoskeletal tension could activate integrin mechanically, as discussed in the next chapter.

Figures

Figure 4.1

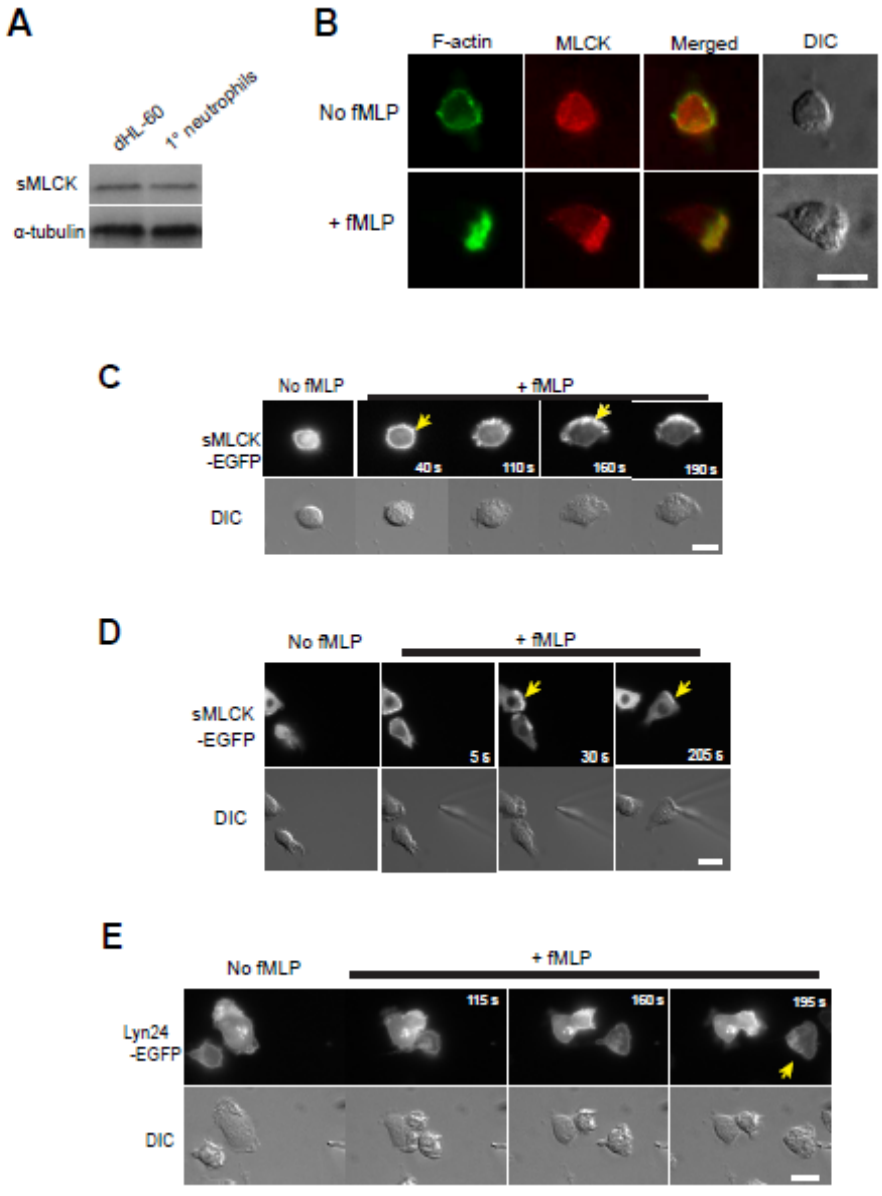

Figure 4.1 (cont.) Short form of MLCK is expressed and recruited to the leading edge in chemotaxing neutrophils

(A) Western blotting of primary human neutrophils and dHL-60 cells with mAbs specific for MLCK. α-tubulin was used as a loading control. (B) dHL-60 cells plated on fibronectin-coated coverslips were stimulated for 2 min with 1 μM fMLP, fixed with 3.7 % paraformaldehyde and stained with a specific anti-MLCK antibody (red) and Alexa fluor 488-conjugated phalloidin (green). The polarized distribution of endogenous MLCK was observed in 188 out of 269 polarized cells. (C) dHL-60 cells were transfected with sMLCK-EGFP and exposed for the indicated times to the uniform concentration of fMLP (1 μM). sMLCK-EGFP fluorescence and the corresponding DIC images are shown. Arrows point to the recruitment of sMLCK-EGFP. n = 31 cells. (D) dHL-60 cells were transfected with sMLCK-EGFP and exposed for the indicated times to 10 μM fMLP from a micropipette. sMLCK-EGFP fluorescence and corresponding DIC images are shown. n > 15 cells. Bars = 10 μm. Arrows point to the recruitment of sMLCK-EGFP. Movie of the cells in (D) is available (Supplementary Movies S10 and S11). (E) dHL-60 cells were transfected with Lyn24-GFP and stimulated by a micropipette containing 10 μM fMLP for the indicated times. GFP fluorescence and the corresponding DIC images are shown. The arrows points to a migrating cell with uniform distribution of Lyn24-GFP. Bar, 10 μm.

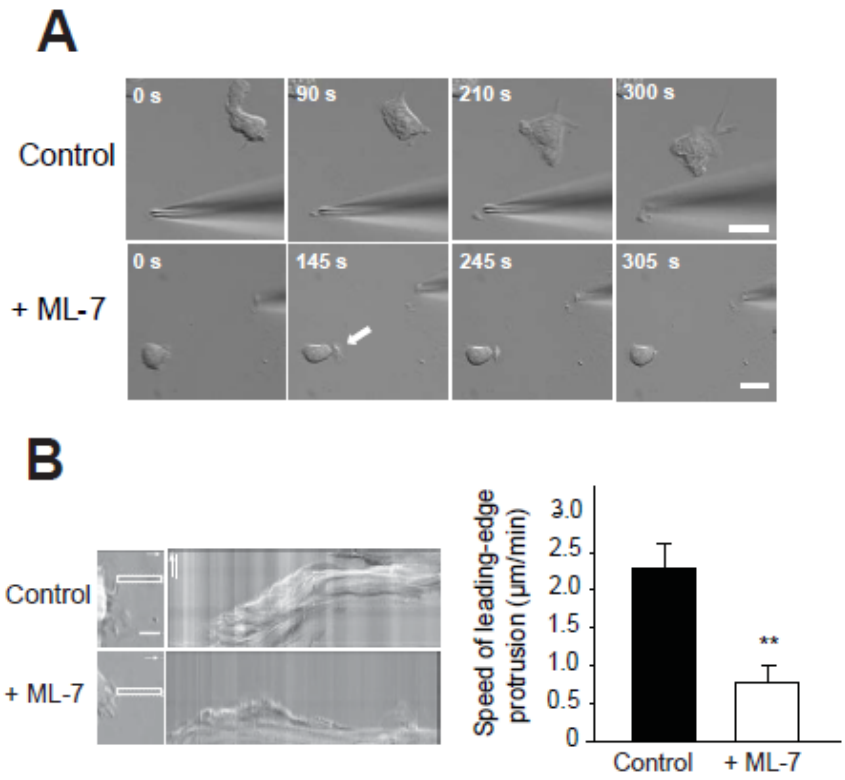

Figure 4.2 MLCK inhibition reduces stability of the leading edge in dHL-60 cells
(A) dHL-60 cell treated with ML-7 (25 μM, 30 min) was exposed to a point source of 10 μM fMLP for the times indicated (bottom panel). The cell fails to migrate to the micropipette and shows poorly developed pseudopod (white arrow). Untreated dHL-60 cell (top panel) with well-developed, stable pseudopod is shown. Bars=10 μm. (B) DIC kymographs (left) of a dHL-60, untreated or treated with ML-7, migrating toward an fMLP (10 μM)-containing micropipette. The dotted rectangles indicate the regions of the cell used to generate the kymographs (prior to fMLP stimulation). The actual lengths of the rectangles are 20 μm in the direction of the arrow. Left panel: scale bar=1 μm. Right panel: scale bars = 5 μm. Arrows indicate the direction of protrusion. 5 min of migration was recorded. The speed of leading-edge protrusion was calculated based on the kymographs (right). The values are means ± SEM (n = 34 for control, and 32 for cells treated with ML-7). Asterisks indicate that the value for cells with ML-7 treatment differs from the corresponding control by $P < 0.0001$.

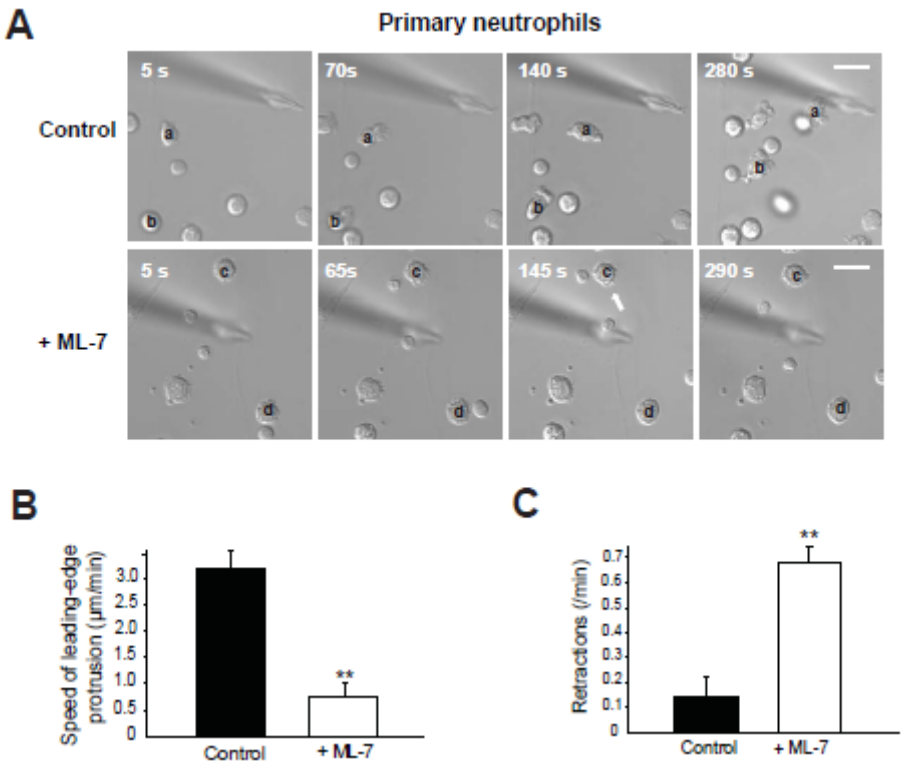

Figure 4.3 MLCK inhibition reduces stability of the leading edge in primary neutrophils

(A) Primary neutrophils were pretreated with or without ML-7 (25 μM, 30 min) prior to the exposure to an attractant supplied by a micropipette containing 10 μM fMLP. The four images in each row show the positions of representative cells (each identified with a superimposed letter) after the indicated times of exposure to fMLP. The white arrow points to the poorly-developed leading edge. Scale bar, 10 μm. (B and C) Speed of protrusion (B) and retraction frequency (C) of the leading edge in primary neutrophils responding to a gradient of fMLP delivered by a micropipette. Cells were pretreated with or without ML-7. The value are means ± SEM (n = 21 for control, 22 for cells treated with ML-7). Student t tests compared data between experimental groups. Results significantly different from those of control are indicated by asterisks (**; $p < 0.001$).

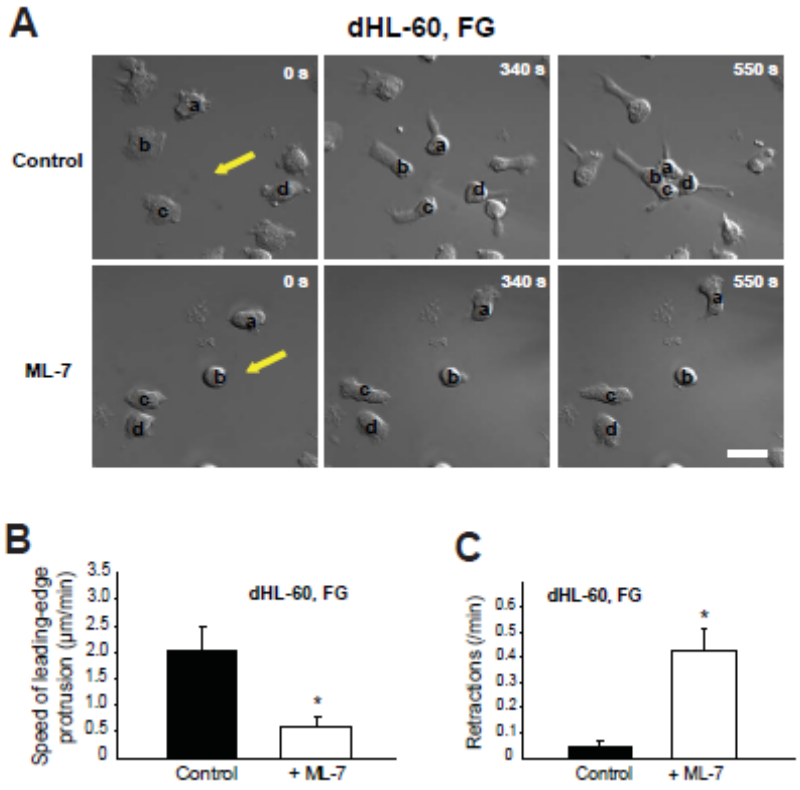

Figure 4.4 MLCK inhibition impairs stability of the leading edge in neutrophils crawling on fibrinogen

(A) Before exposure to attractant supplied by a micropipette containing 10 μM fMLP, cells plated on fibrinogen (denoted as FG) were not pretreated (control) or pretreated with ML-7 (25 μM, 30 min). The three images in each row show the positions of individual cells (each identified with a superimposed letter) after the indicated times of exposure to fMLP. The yellow arrows point to the position of micropipettes, which are out of focus. Scale bar, 10 μm. (B and C) Speed of protrusion (B) and retraction frequency (C) of the leading edge in cells on fibrinogen responding to a gradient of fMLP delivered by a micropipette. dHL-60 cells were not pretreated (control) or pretreated with ML-7. The value are means ± SEM (n = 22 for control, 21 for cells treated with ML-7. Student t tests compared data between experimental groups. Asterisks indicate that the value for cells with ML-7 treatment differs from the corresponding control by $P < 0.0001$.

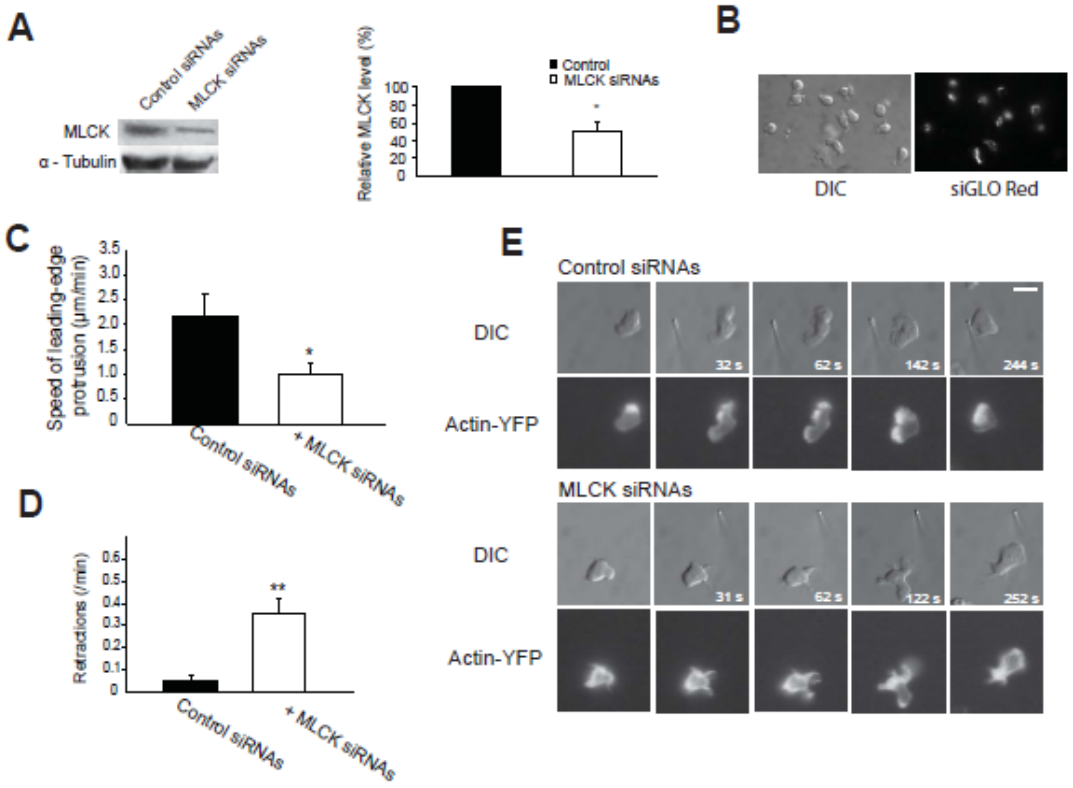

Figure 4.5 MLCK depletion disrupts the stability of the leading edge in neutrophils
(A) dHL-60 cells were transfected with pooled siRNAs which are specifically targeting human MLCK or non-targeting and blotted for MLCK (left panel). α-tubulin is a loading control. Right panel: relative level of endogenous MLCK is measured after transfecting each siRNA constructs. Values are means ± SEM (n = 3). Results significantly different from those of control are indicated by asterisks (*, $p < 0.05$). (B) dHL-60 cells were co-transfected with siGLO Red and pooled siRNAs that are either non-targeting or specifically targeting human MLCK at the ratio of 1:5. 48 hrs after transfection, pictures were taken to check the transfection efficiency of siRNAs into dHL-60 cells. Only images of cells co-transfected with siGLO and non-targeting siRNAs are shown. Bar, 10 μm. (C and D) dHL-60 cells which were transfected with pooled siRNAs that are either non-targeting or specifically targeting human MLCK were exposed to a chemotactic gradient delivered from a micropipette containing 10 μM fMLP for 5 min. Speed of protrusion (C) and retraction frequency (D) of the leading edge in cells responding to the gradient throughout the observed time period. The results are shown in the graph (n = 49 for non-targeting siRNA-transfected cells, 56 for MLCK-specific siRNA-transfected cells). Results significantly different from those of control are indicated by asterisks (*, p

Figure 4.5 (cont.) < 0.001; **; p < 0.0001). MLCK depletion caused similar protrusion and migration defects when cells were stimulated on fibrinogen (data not shown). (E) dHL-60 cells co-transfected with actin-YFP and siRNAs (either non-targeting or specifically targeting human MLCK) were exposed to a chemotactic gradient delivered from a micropipette containing 10 μM fMLP for the times indicated. Fluorescence images of actin-YFP and the corresponding DIC images are shown. (n = 14 for non-targeting siRNA-transfected cells, 11 for MLCK-specific siRNA-transfected cells). All scale bars = 10 μm.

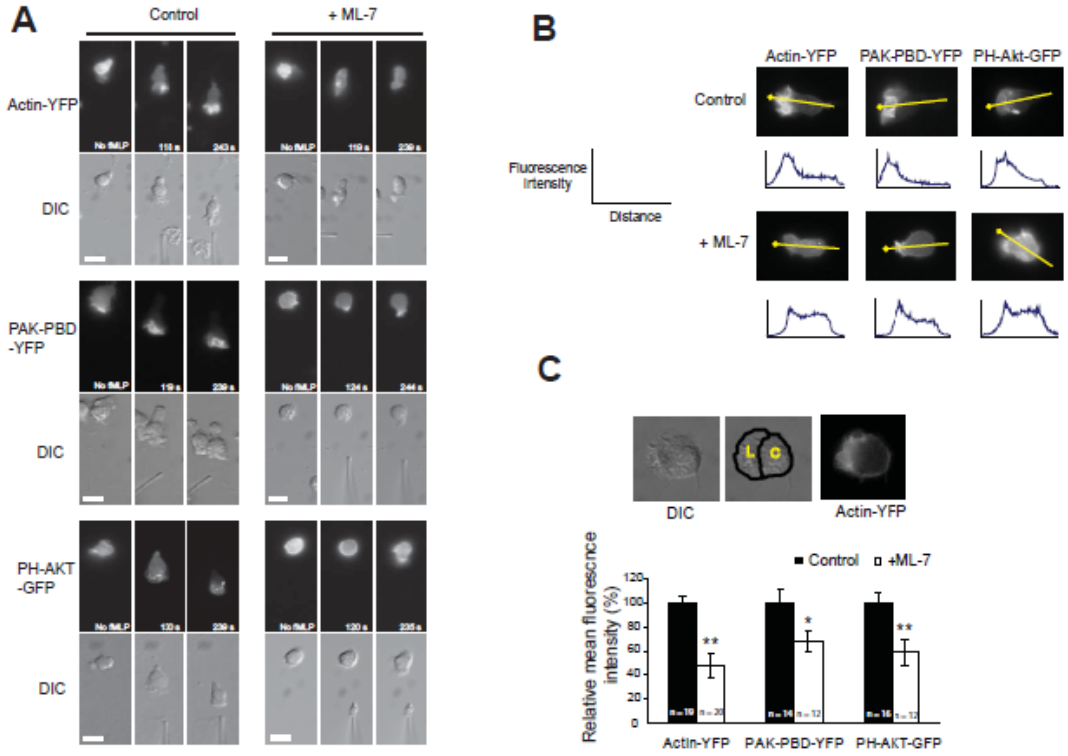

Figure 4.6 MLCK inhibition impairs stable accumulation of frontness signals at the leading edge

(A) dHL-60 cells transfected with actin-YFP (top), PAK-PBD-YFP (middle), or PH-AKT-GFP (bottom) and pretreated with or without ML-7 (25 μM, 30 min) were exposed to an fMLP (10 μM)-containing micropipette and allowed to migrate for the times indicated. Fluorescence of each probe and the corresponding DIC images are shown. Bar, 10 μm. (B) Spatial distribution and line profiles of actin-YFP, PAK-PBD-YFP, and PH-AKT-GFP gradients in dHL-60 cells exposed to fMLP (10 μM), delivered from a micropipette (white dot indicates the beginning of the measurement) for ~ 240 s. Cells were not pretreated (top) or were pretreated with ML-7 (bottom). A graph below each image plots fluorescence intensity of each probe (y axis) versus distance (x axis) for the corresponding cell. (C) Relative accumulation of actin-YFP, PAK-PBD-YFP, and PH-AKT-GFP at the leading edge of dHL-60 cells exposed to fMLP (10 μM), delivered from a micropipette. Leading edge (L) in fluorescence image was demarcated by the corresponding DIC image and the rest of the cell was defined as cell body (C). Cells were pretreated with or without ML-7. For control cells, 3 min after the attractant exposure was chosen for analysis. For treated cells, a time point when the pseudopod extension is at its peak was selected. Each bar in the graph below represents the ratio of mean fluorescence intensity between the leading edge and cell body. Values are normalized to the ratio of mean fluorescence intensity in control cells (=100%) and are means ± SEM (n is shown within each bar). Results significantly different from those of control are indicated by asterisks (*, $p < 0.001$; **; $p < 0.0001$).

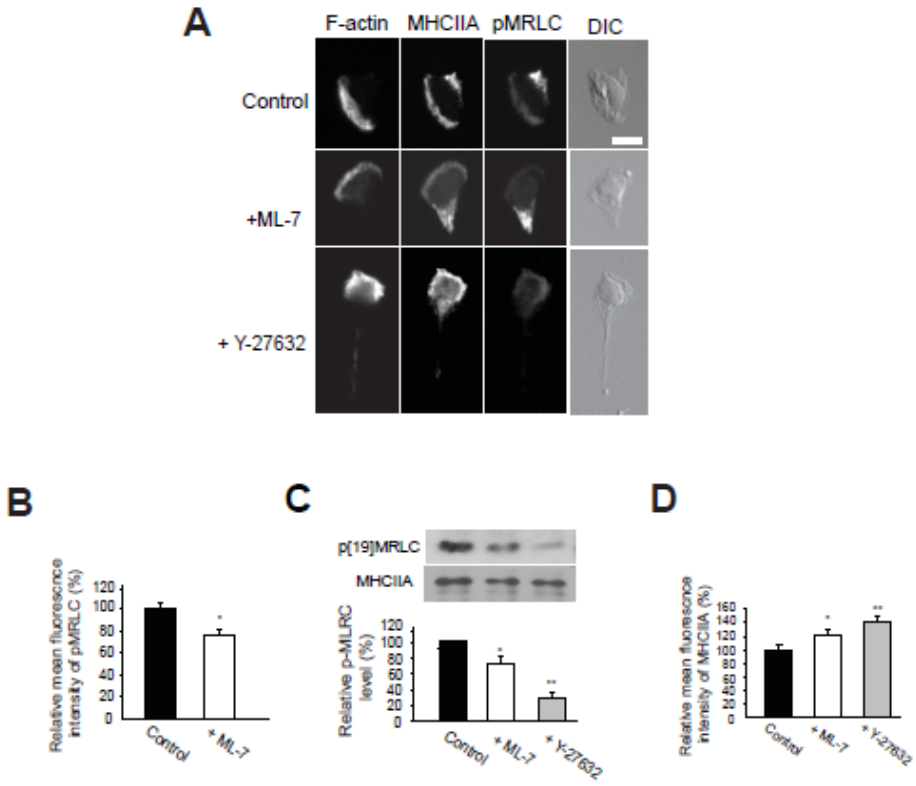

Figure 4.7 MLCK inhibition/depletion impairs myosin II activity at the leading edge (A) dHL-60 cells not pretreated or pretreated with ML-7 (25 μM, 30 min) or Y-27632 (30 μM, 30 min) were stimulated for 3 min by a uniform concentration of 1 μM fMLP. Cells were fixed with 3.7 % paraformaldehyde and stained with the anti-MHCIIA antibody, anti-p[Ser19]MRLC antibody, and rhodamine-conjugated phalloidin. The corresponding DIC images are also shown. Bar, 10 μm. (B) The distribution of p[Ser19]MRLC in dHL-60 cells with or without ML-7 treatment was analyzed. The mean fluorescence of p[Ser19]MRLC staining at the leading and the trailing edge of cells was determined using Image J software, and the ratios between the leading and the trailing edge (i.e., mean fluorescence intensity at the leading edge/mean fluorescence intensity at the trailing edge) are shown. Values were normalized to the ratio (=100%) in control cells and are means±SEM (n = 40 for control, and 30 for cells treated with ML-7). Student t tests compared data between experimental groups. Results significantly different from those of control are indicated by asterisks (*; $p < 0.001$). (C) Western blot of p[Ser19]MRLC. dHL-60 Cells were pretreated with no inhibitors, ML-7 (25 μM, 30 min pretreatment), or Y-276322 (30 μM, 30 min) before exposure to fMLP for 2 min in suspension. A typical blot is shown in the top panel, and quantification of blots from four

Figure 4.7 (cont.) separate experiments is shown in the bottom panel. Each bar represents the mean±SEM (error bars). All values were normalized to the signal (=100%) detected without the inhibitors. Asterisks indicate that the value for cells treated with M-7 or Y-27632 differs statistically from the control (*, $p<0.01$; **, $p<0.001$). Total MHCIIA levels were unaltered with the treatments and used for equal loading in the different lanes. (D) The distribution of total MHCIIA in control dHL-60 cells and cells pretreated with ML-7 or Y-27632 was analyzed. The mean fluorescence of MHCIIA staining at leading and trailing edges was assessed by Image J software, and the ratios between leading and trailing edges are shown. Values were normalized to the ratio (=100%) in control cells and are means ± SEM (n = 40 for control, 30 for cells treated with ML-7, and 25 for cells treated with Y-27632). Results significantly different from those of control are indicated by asterisks (*, $p < 0.05$; **; $p < 0.001$).

Figure 4.8

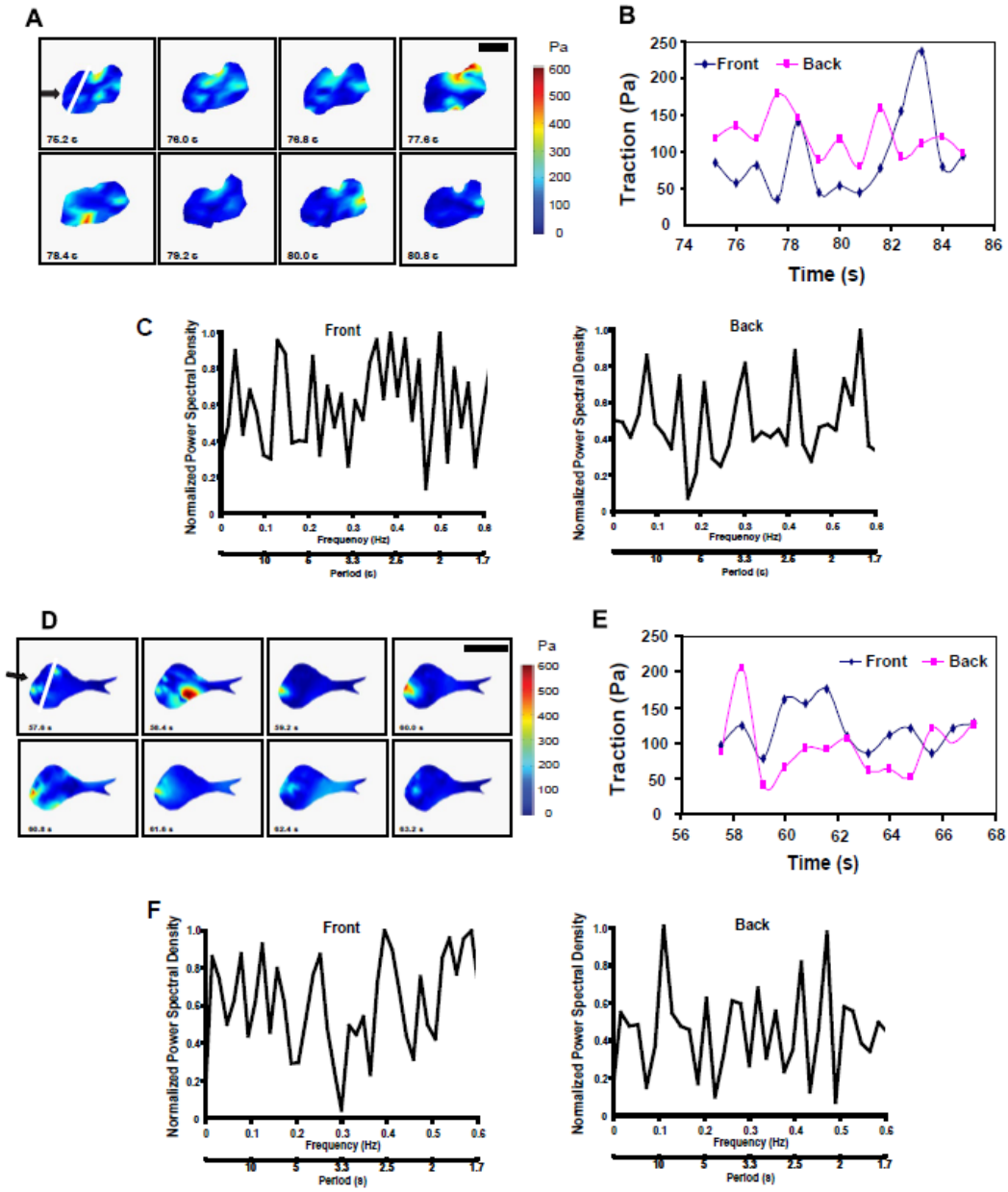
A
Pa
600
500
400
300
200
100
0
75.2 s
76.0 s
76.8 s
77.6 s
78.4 s
79.2 s
80.0 s
80.8 s
B
Front
Back
Traction (Pa)
Time (s)
C
Front
Back
Normalized Power Spectral Density
Frequency (Hz)
Period (s)
D
E
F

Figure 4.8 (cont.) Localization-specific myosin activities are necessary for tractions in neutrophils

(A) dHL-60 cells depleted of MLCK were allowed to migrate toward chemoattractant-containing micropipette (fMLP, 10 μM) on a fibronectin-coated elastic polyacrylamide gel for the indicated times. Traction maps of the cell are shown. Pseudocolor bar representing tractions is given in Pascal (Pa). Scale bar = 5 μm. The leading edge (within the first 2.2 μm of the cell) is marked by a white line (see Supplementary Methods). The image series shows part (5.6 sec) of the whole migratory response. Cells treated with ML-7 exhibited similar responses. Cells treated with ML-7 or MLCK-specific siRNAs migrated at 1.1 μm/min on the elastic gel. The movie of the cell in (A) is available in the Appendix. (B) Time series of traction maps from (A) (with five additional time points) was analyzed by a customized MATLAB program to determine the average traction force in both leading (front) and trailing edges (back) of the cells in a time-dependent manner. The graph shows part (~9.6 sec) of the whole migratory response. x axis indicates time in sec. y axis is in Pascal (Pa). (C) PSD plots of tractions at the leading (left panel) and the trailing edge (right panel) of a migratory cell with MLCK depleted. The whole migratory response was analyzed. y axis represents the power spectral density normalized to the highest peak value (=1). x axis shows the oscillation frequency (Hz) (top) or period (s) (bottom). Cells pretreated with ML-7 exhibited similar response (not shown). 10 cells were analyzed, and a representative cell is shown. Additional plots for ML-7 treatment and MLCK depletion are shown in Figure 4.9A and Figure 4.9B. (D) dHL-60 cells pretreated with Y-27632 (30 μm, 30 min) were allowed to migrate toward chemoattractant-containing micropipette (fMLP, 10 μM) on a fibronectin-coated elastic polyacrylamide gel for the indicated times. Traction force maps of the cell are shown. Pseudocolor bar representing traction force is given in Pascal (Pa). Scale bar = 10 μm. The leading edge (within the first 3 μm of the cell) is marked by a white line (see Materials and Methods). The image series shows part (5.6 sec) of the whole migratory response. (E) Time series of traction force maps from (D) (with five additional time points) was analyzed by a customized MATLAB program to determine the average traction force in both leading (front) and trailing edges (back) of the cells in a time-dependent manner. The graph shows part (~9.6 sec) of the whole migratory response. x axis indicates time in sec. y axis is in Pascal (Pa). (F) PSD plots of tractions at the leading (left panel) and the trailing edge (right panel) of a migratory cell pretreated with Y-27632. The whole migratory response was analyzed. y axis represents the power spectral density normalized to the highest peak value (=1). x axis shows the oscillation frequency (Hz) (top) or period (s) (bottom). 8 cells were analyzed, and a representative cell is shown. Additional plots are shown in Figure 4.9C.

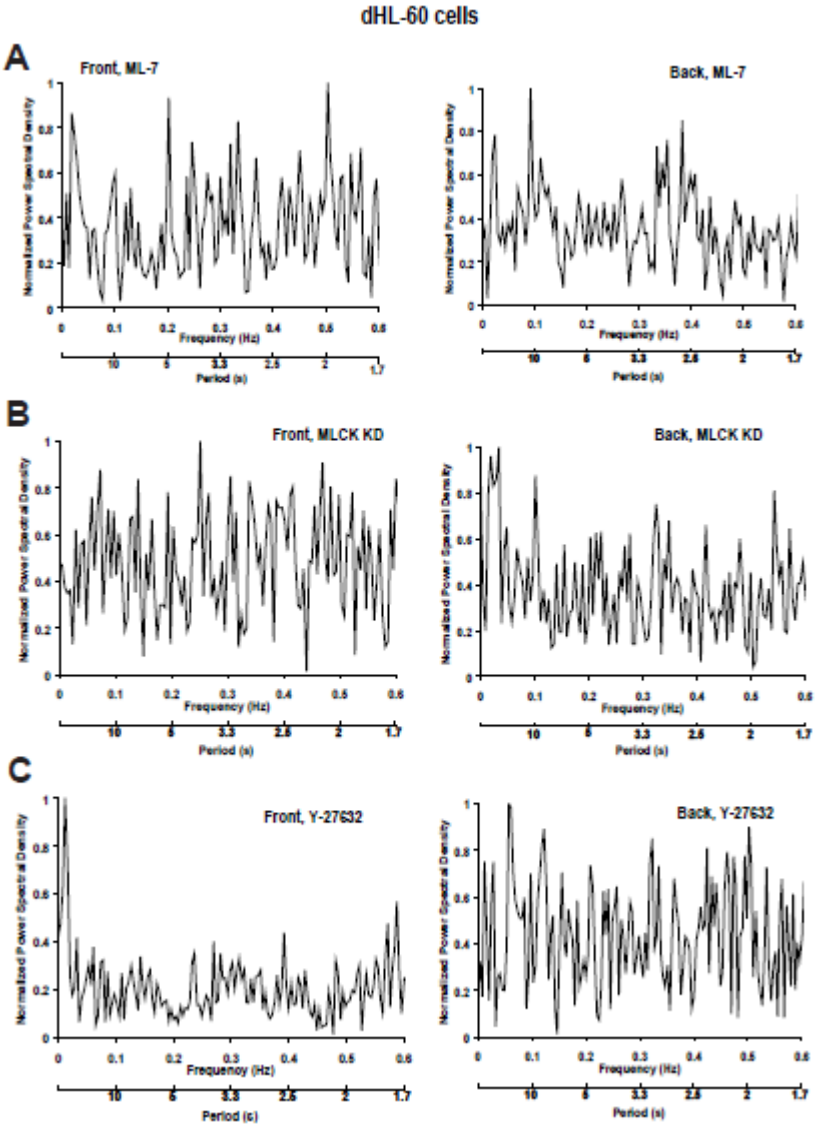

Figure 4.9 Inhibition (or depletion) of MLCK or ROCK abolishes periodicity of traction in dHL-60 cells

PSD plots of tractions at the leading (left panel) and the trailing edge (right panel) of three dHL-60 cells pretreated with ML-7 (25 μM, 30 min) (A), with MLCK depleted (B) and pretreated with Y-27632 (100 μM, 30 min) (C). Tractions values from three cells were analyzed and combined in one plot. See Figure 4.8 legends for more details.

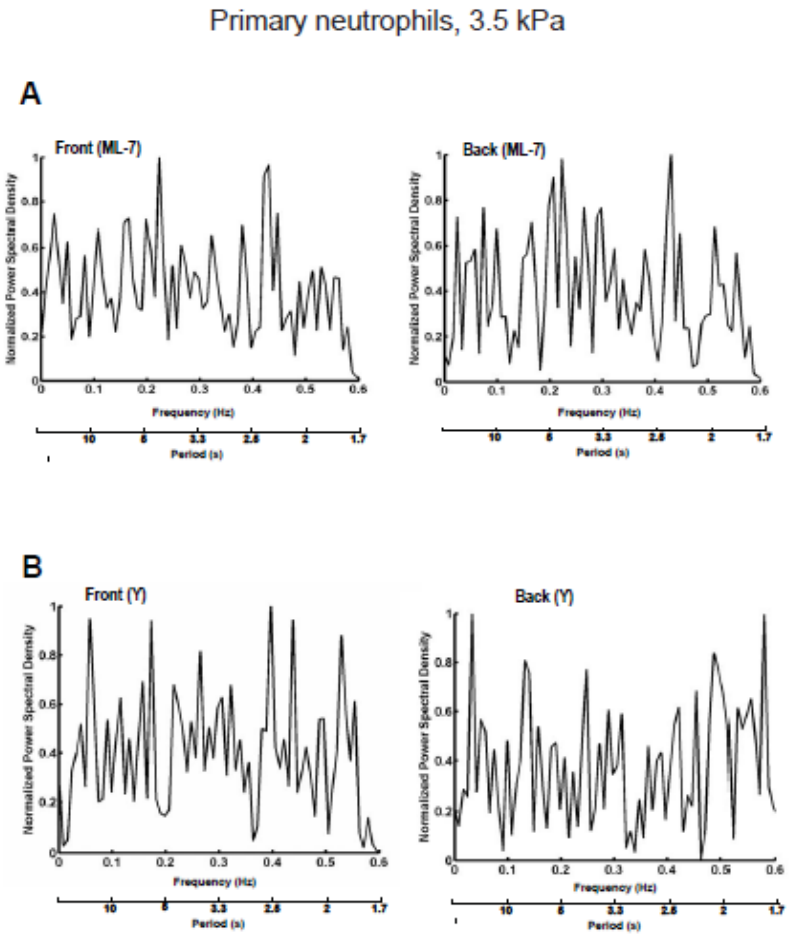

Figure 4.10 Inhibition of MLCK or ROCK abolishes periodicity of traction in primary neutrophils

PSD plots of tractions at the leading (left panel) and the trailing edge (right panel) of primary neutrophils pretreated with ML-7 (25 μM, 30 min) (A), or Y-27632 (100 μM, 30 min) (B). 6 cells were analyzed for each treatment, and a representative cell is shown. Cells were on a substrate of 3.5 kPa stiffness.

Figure 4.11

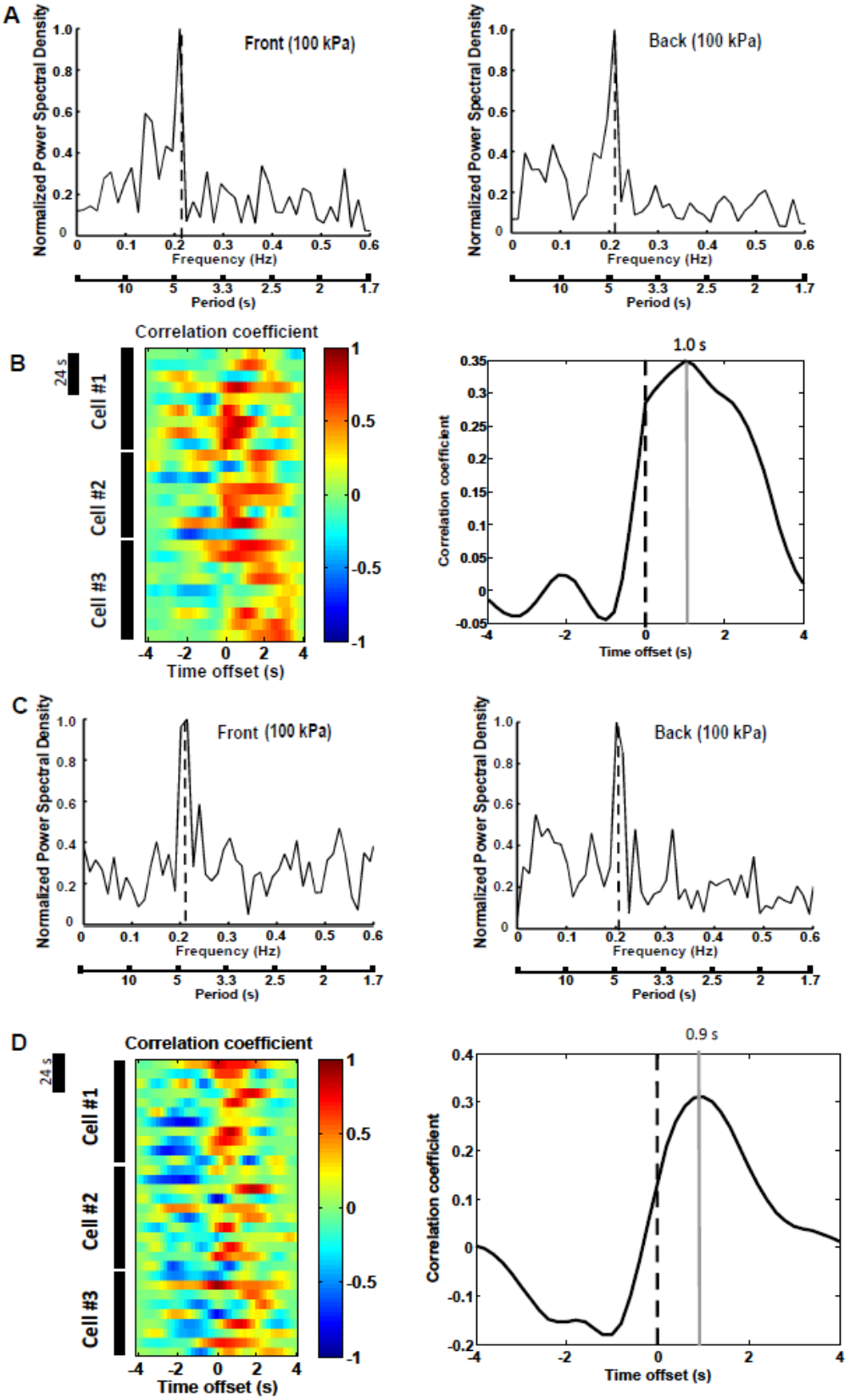
A
Front (100 kPa)
Back (100 kPa)
Normalized Power Spectral Density
Frequency (Hz)
Period (s)
B
Correlation coefficient
24 s
Cell #1
Cell #2
Cell #3
Time offset (s)
1.0 s
Correlation coefficient
C
Front (100 kPa)
Back (100 kPa)
D
Correlation coefficient
0.9 s

Figure 4.11 (cont.) The pattern and regulation of tractions in neutrophils on a stiffer substrate

(A) PSD plots of tractions at the leading (left panel) and the trailing edge (right panel) of a migratory primary neutrophil. PSD plots were generated based on the results from Fourier analysis of the traction values. y axis represents the power spectral density normalized to the highest peak value (=1). x axis shows the oscillation frequency (Hz) (top) or period (s) (bottom). Primary cells were allowed to migrate toward chemoattractant-containing micropipette (fMLP, 10 μM) on a fibronectin-coated polyacrylamide gel (100 kPa) for 4-5 min. 6 cells were analyzed, and a representative cell is shown. (B) Left panel: Cross correlation between tractions at the leading and the trailing edge against time offset during migration for individual primary neutrophils. Dotted lines indicate zero offset. Data from 3 representative cells are shown. Time bar = 24 s. Right panel: Summary of time offsets between leading edges and trailing edges (n=6 cells) in primary cells. (C) PSD plots of tractions at the leading (left panel) and the trailing edge (right panel) of a migratory primary neutrophil pretreated with Y-27632 (30 μM, 30 min). PSD plots were generated based on the results from Fourier analysis of the traction values. y axis represents the power spectral density normalized to the highest peak value (=1). x axis shows the oscillation frequency (Hz) (top) or period (s) (bottom). Cells were allowed to migrate toward chemoattractant-containing micropipette (fMLP, 10 μM) on a fibronectin-coated polyacrylamide gel (100 kPa) for 4-5 min. 6 cells were analyzed, and a representative cell is shown. (D) Left panel: Cross correlation between tractions at the leading and the trailing edge against time offset during migration for individual Y-27632-treated primary neutrophils. Dotted lines indicate zero offset. Data from 3 representative cells are shown. Time bar = 24 s. Right panel: Summary of time offsets between leading edges and trailing edges (n=6 cells) in Y-27632-treated primary cells.

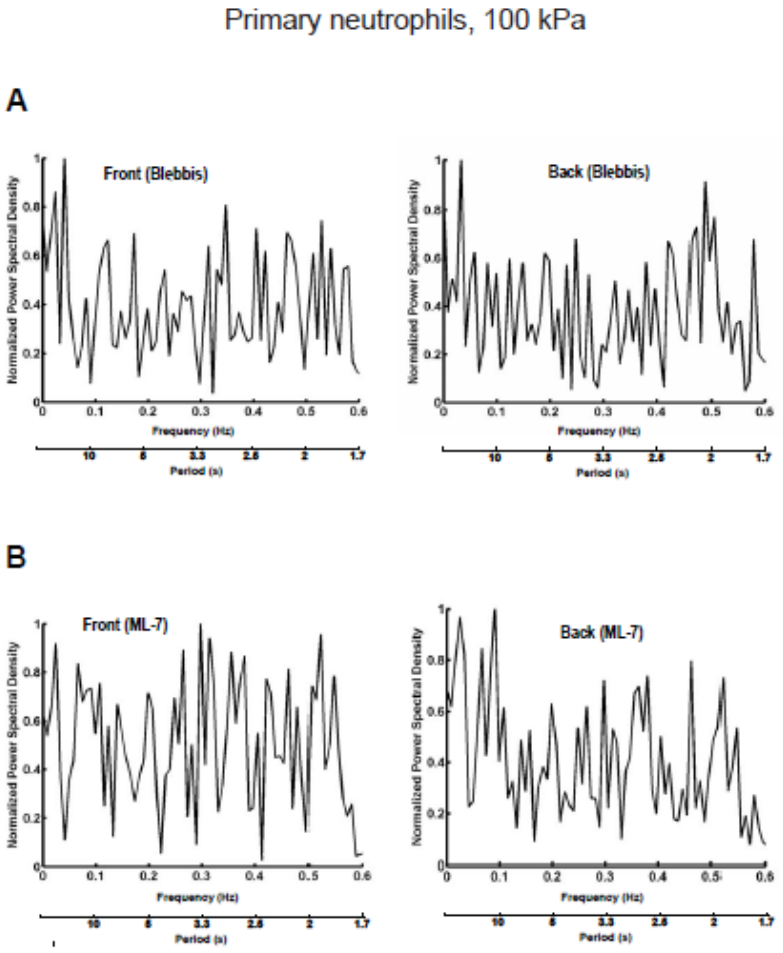

Figure 4.12 Inhibition of myosin II or MLCK abolishes the periodicity of traction in primary neutrophils on a stiffer substrate

PSD plots of tractions at the leading (left panel) and the trailing edge (right panel) of a migratory primary neutrophil pretreated with ML-7 (25 μM, 30 min) (A) or Blebbistatin (100 μM, 30 min) (B). Cells were allowed to migrate toward chemoattractant-containing micropipette (fMLP, 10 μM) on a fibronectin-coated polyacrylamide gel (100 kPa) for 4-5 min. 6 cells were analyzed for each condition, and a representative cell is shown.

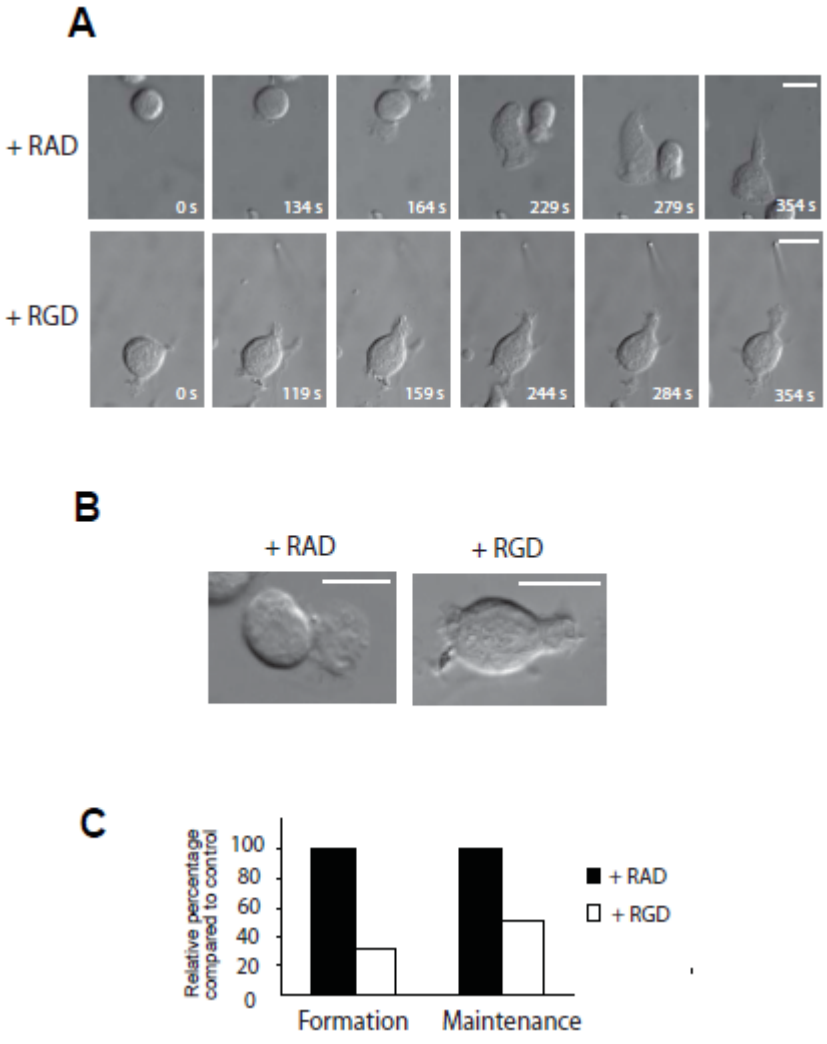

Figure 4.13 Inhibition of adhesion prevents leading-edge establishment and stability
(A) A dHL-60 cell bathed in RGD peptides (50 µg/ml) was exposed to a point source of fMLP (10 µM in the micropipette) for the times indicated (bottom). The cell fails to migrate to the micropipette and shows poorly developed pseudopod. Compare this response to that of a dHL-60 cell (top) in RAD (50 µg/ml)-containing buffer which shows well-developed, stable pseudopod. (B) Higher magnification DIC images of two migrating cells show characteristic shapes of the leading edge either with RAD treatment (left) or with RGD treatment (right). (C) dHL-60 cells bathed in either RAD or RGD peptides (50 µg/ml) were exposed to a chemotactic gradient delivered from a micropipette containing 10 µM fMLP for 10 min. The cells were assessed for their ability to establish or maintain polarity toward the micropipette throughout the observed time period. The result is shown in the graph (n = 43 for RAD-treated cells, 48 for RGD-treated cells). All scale bars = 10 µm.

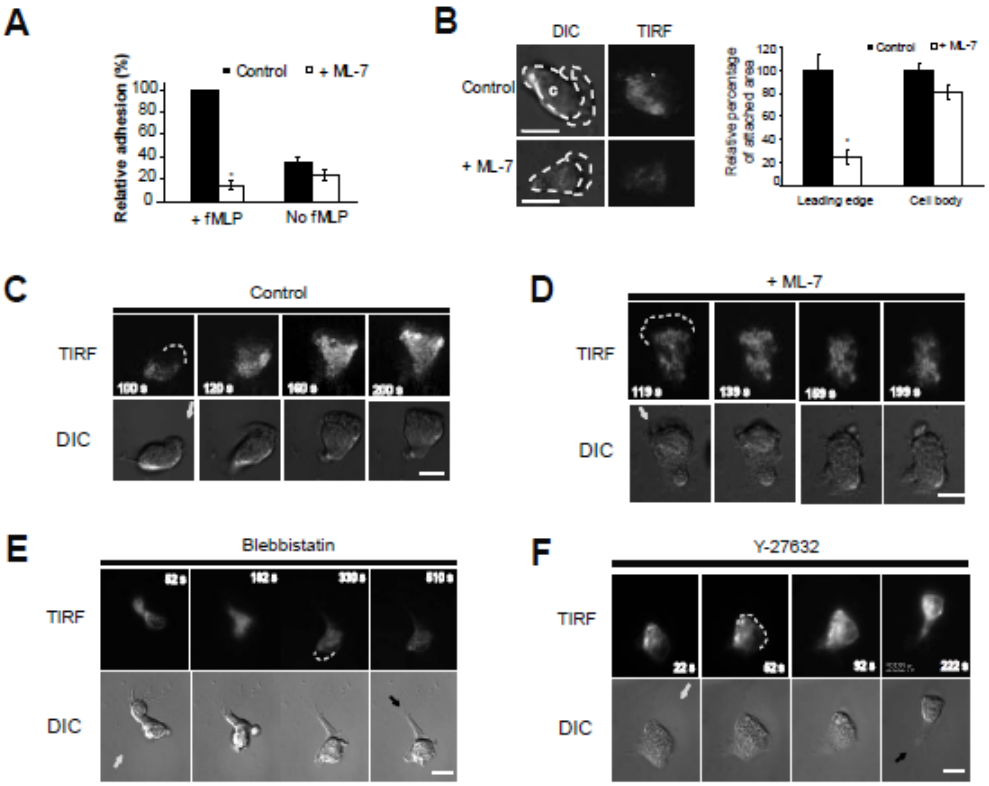

Figure 4.14 MLCK inhibition impairs attachment of the leading edge in neutrophils
(A) dHL-60 cells pretreated with (25 µM, 30 min) or without ML-7 were not stimulated or stimulated in suspension by 100 nM fMLP and allowed to adhere to fibronectin-coated surface for 30 min, after which the degree of cell adhesion was assessed. Values were normalized to adhesion in control cells (=100%) with fMLP and are means±SEM (n=4). Results significantly different from those of control are indicated by asterisks (*, $p < 0.001$). (B) Assessment of adhesion area in leading edge and cell body in control and ML-7-treated cells transfected with EGFP-α5-integrin and exposed to a point source of 10 µM fMLP. Cell images were from Figure 4.14 (C) and (D). Left panel: The time point at which leading edge protrusion of individual cell‘s was maximal was selected for analysis. Leading edge (denoted as “L”) in TIRF image was demarcated by the corresponding DIC image, and the rest of the cell was defined as Cell body (denoted as “C”). Right panel: fluorescence intensities of the leading edge and the cell body in the TIRF images of control and ML-7-treated cells were determined with Image J, and the resulting values were used to quantify cell attachment of the both leading edge and the cell body. The plot shows the relative values in each region compared to control (=100%) in the presence of fMLP stimulation. Values are means±SEM (n=13 for control, 11 for cells treated with ML-7). Results significantly different from those of control are

Figure 4.14 (cont.) indicated by asterisks (*; $p < 0.0001$). (C-F) dHL-60 cells were transfected with EGFP-α5-integrin and exposed to a point source of 10 μM fMLP (from micropipette) for the indicated times. TIRF (488 nm) and the corresponding DIC images are shown. Cells were not pretreated (C) pretreated with ML-7 (D), Blebbistatin (E) and Y-27632 (F). Leading-edge attachment of control cells was indicated by the GFP fluorescence; nearly no signals were detected at the leading edges in cells treated with ML-7 or Blebbistatin. Leading edges in the TIRF images are marked by white dotted lines. White arrows indicate the direction of chemoattractant gradient. Black arrows point to the long stretched trailing edges.

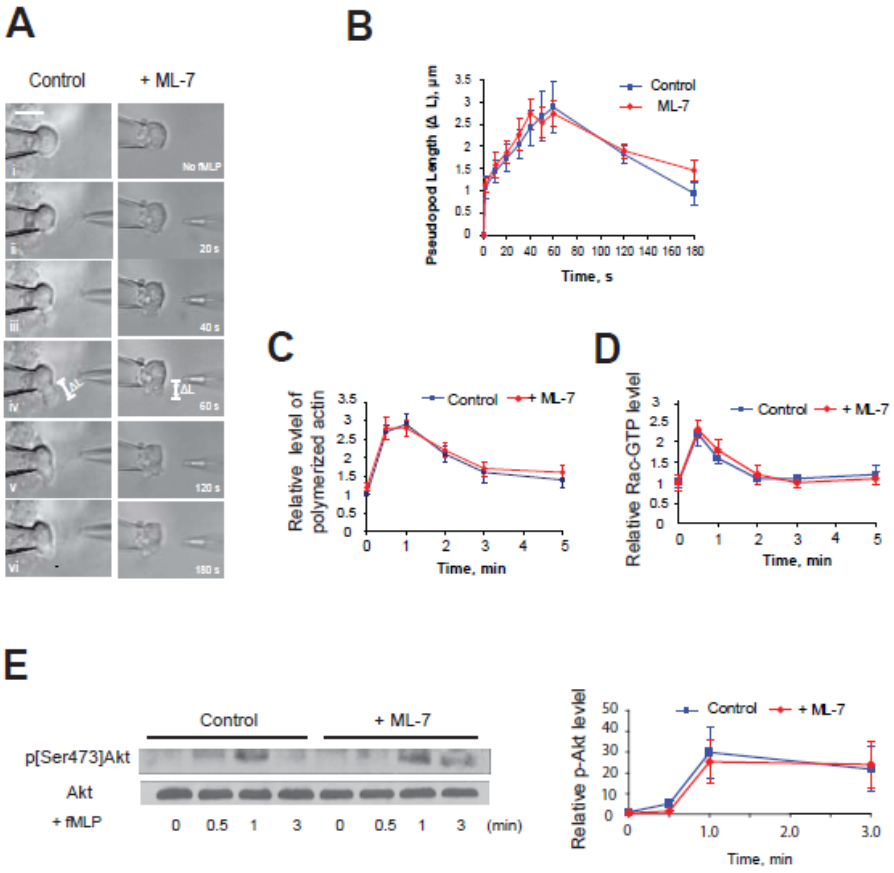

Figure 4.15 MLCK is not required for protrusion per se

(A) A single, non-stimulated dHL-60 cell, pretreated with or without ML-7 (25 μM, 30 min), was held with a pipette and exposed to a gradient from 10 μM fMLP from a delivery pipette. Before exposure to fMLP, the cell was spherical (i). Within 20 s, a pseudopod started to grow (ii). The pseudopod extended until a maximal length was reached (iii and iv), and then it started to retract (v and vi). Bar, 10 μm. (B) The growth of pseudopod as a function of time. Pseudopod formation was stimulated with delivery of 10 μM fMLP from a pipette as shown in (A). Chemoattractant delivery started at time 0. Values are means±SEM (n=6). (C) Quantification of F-actin polymerization. Cells pretreated with or without ML-7 were stimulated with fMLP (1 μM) for various times in suspension and fixed for staining with rhodamine-phalloidin. Fluorescence in stained cells was determined by flow cytometry. Values are means ± SEM (n = 4). (D) Quantification of Rac-GTP in dHL-60 cells with or with ML-7 treatment. Cells were pretreated with ML-7, stimulated with fMLP (1 μM) for times indicated and lysed. The level of Rac-GTP was determined by the use of an absorbance-based Rac G-LISA kit. The y axis represents relative absorbance normalized to the signal (=1) detected in the control cells without ML-7 treatment. Each bar represents the mean±SEM (error bars) (n =4). (E) dHL-60 cells pretreated with or without ML-7 were stimulated for indicated times in suspension and lysed. Akt phosphorylation (Ser473) was assessed by western blotting. Values are normalized to the level in control cells without fMLP stimulation (=1) and are means±SEM (n=8). Representative blots for phospho- and total Akt are shown.

Figure 4.16

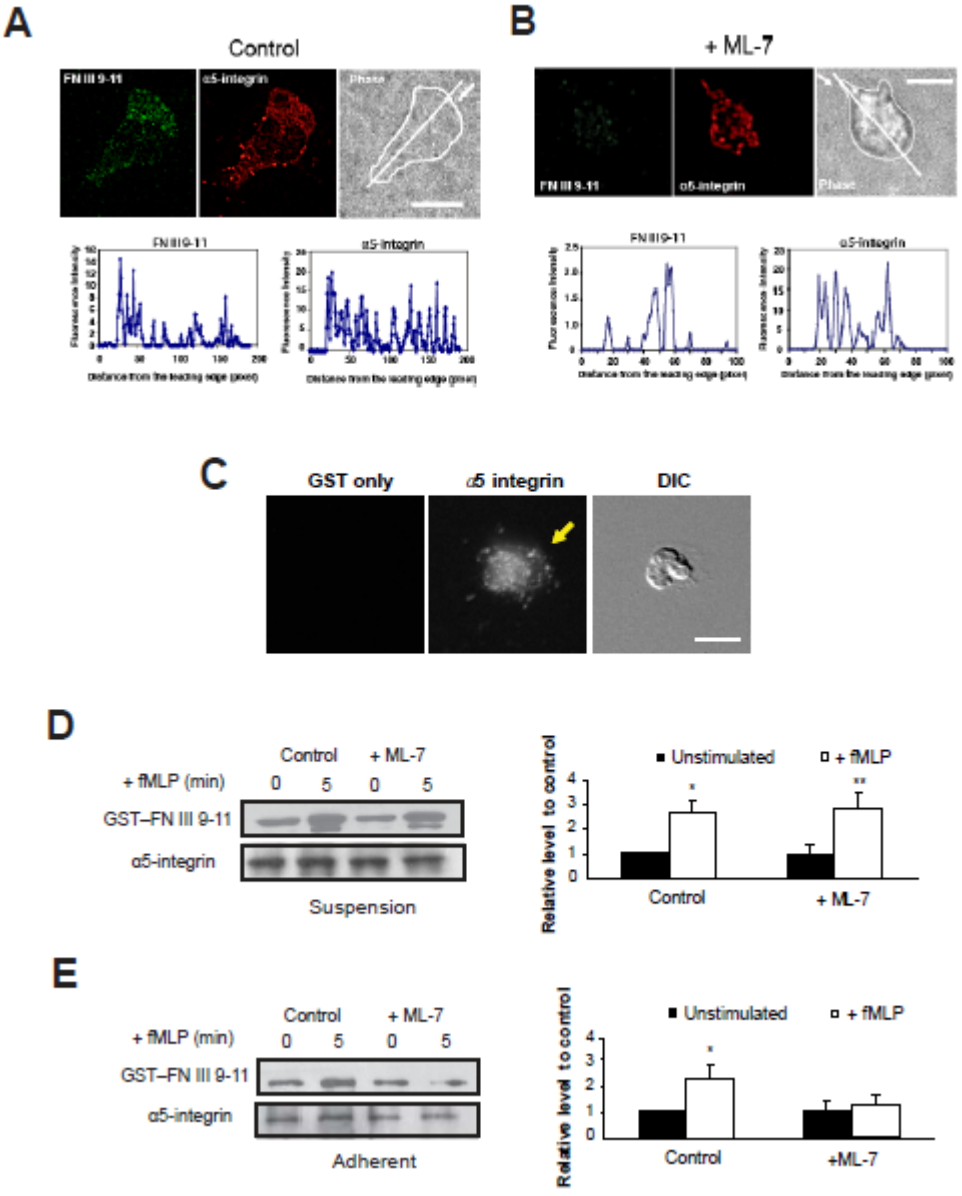
A
Control
FN III 9-11
α5-integrin
Phase
FN III 9-11
α5-integrin
B
+ ML-7
FN III 9-11
α5-integrin
Phase
FN III 9-11
α5-integrin
C
GST only
α5 integrin
DIC
D
Control
+ ML-7
+ fMLP (min)
0
5
0
5
GST–FN III 9-11
α5-integrin
Suspension
Unstimulated
+ fMLP
Relative level to control
Control
+ ML-7
E
Control
+ ML-7
+ fMLP (min)
0
5
0
5
GST–FN III 9-11
α5-integrin
Adherent
Unstimulated
+ fMLP
Relative level to control
Control
+ML-7

Figure 4.16 (cont.) MLCK controls neutrophil adhesion and integrin activation
(A, B) Upper panel: Localization of activated α5β1 integrins in polarized neutrophils pretreated with or without ML-7 (25 μM, 30 min). dHL-60 cells pretreated with or without ML-7 were plated on fibronectin-coated coverslips and stimulated for 3 min by 1 μM fMLP. After washing, cells were fixed with 3.7 % paraformaldehyde, incubated with GST-FN III_{9-11} (50 μg/ml) for 15 min at 37°C, and stained with an anti-GST antibody and anti-α5-integrin antibody. Fluorescent (red: α5-integrin; green: activated integrin) and phase contrast images were collected by using confocal fluorescence microscopy. The images of a representative cell for each condition are shown (n=20 for control, n=17 for ML-7 treatment). Arrows indicate the leading edge. White line indicates the path along which line profile was obtained. The weak signals for GST-FN binding may be attributed to the relative low levels of activated α5β1-integrin in the cells. Bar, 10 μm. Lower panel: Line profiles of GST-FN III_{9-11} and α5-integrin fluorescence in cells shown in the upper panel. The graphs plot fluorescence intensity of each protein (y axis; in arbitrary unit) versus distance (x axis in pixels) along the white line on the phase contrast image of the cells. (C) dHL-60 cells were fixed, incubated with GST, fixed and stained with an anti-GST antibody and anti-α5-integrin antibody. The procedure was performed as described in Figure 4.16A-B, except that GST was used. The yellow arrow points to the leading edge. Bar, 10 μm. (D, E) Levels of activated α5β1 integrins in cells with or without ML-7 treatment. dHL-60 cells pretreated with or without ML-7 were stimulated by a uniform concentration of fMLP (100 nM) in either suspension (D) or adhesion conditions (E). After brief washing, cells were incubated with GST-FN III_{9-11} (50 μg/ml) for 30 min at 37°C, washed and lysed. The lysates were probed with an anti-GST antibody. α5-integrin was used as a loading control. A typical blot is shown on the left. The right panel shows quantification of blots from four separate experiments. The y axis represents relative intensities (measured with Image J) with values normalized to the signal (=1) detected in the control cells without ML-7 treatment. Each bar represents the means±SEM (n=4). Results significantly different from those of cells without fMLP stimulation are indicated by asterisks (*, $p < 0.0001$; **; $p < 0.001$).

CHAPTER 5

DISCUSSION

As discussed in the Introduction, traction is essential in cell migration in that it provides driving force for forward movement of cells and yet, there is a paucity of information on the spatiotemporal pattern, regulation and function of traction during neutrophil chemotaxis. Employing traction force microscopy at a much higher temporal resolution in a physiologically more relevant setting than previously reported, we revealed that there is a periodic pattern of traction at the leading and the trailing edges in neutrophils during chemotaxis. We also found the regulatory mechanism of traction in neutrophil chemotaxis in which nonmuscle myosin II and its spatially distinct, upstream kinases are involved. In particular, MLCK-driven contractile forces at the leading edge were found to be important for traction and adhesion, allowing persistent protrusion in neutrophil chemotaxis. Our findings have begun to shed light on the characteristics, mechanisms and functions of traction in neutrophil chemotaxis.

Periodic, out-of-phase pattern of traction in neutrophil chemotaxis

Our results reveal novel mechanical aspects of cell polarity and motility in neutrophils and are summarized in a model (Figure 5.1). We discovered a periodic pattern of tractions at the leading and the trailing edge in a neutrophil-like cell line and primary neutrophils during chemotaxis. This oscillatory pattern has not been documented for any biochemical or mechanical factors in neutrophils during chemotaxis. What might be the function of the periodic tractions? We speculate that the oscillations at the front of the cell may be linked to the cycle of leading edge extension and adhesion. In this scenario, extension of the pseudopod occurs with minimal contact with the ECM substrate and is thus associated with weak tractions. In contrast, strong tractions could result from establishment and stabilization of leading edge attachment. In addition, the traction oscillations at the cell's rear may correspond to periodic contractions that enable the cell to pull the trailing edge forward. A future study examining the link between the

periodic oscillation of traction and the distinct steps in cell migration cycle (i.e., protrusion, adhesion, contraction and tail retraction) during neutrophil chemotaxis is required to test the validity of such hypothesis.

Interestingly, in addition to the periodic patterns, we found that the traction oscillations at the front and the back are out of phase, with the tractions at the front leading those at the back, thus pointing to a timing mechanism that allows neutrophils to coordinate leading edge adhesion and trailing edge de-adhesion to ensure persistent movements. We can only speculate about the molecular mechanism that gives rise to the temporal shift. Chemoattractant-induced activation of MLCK may precede that of p160-ROCK (Figure 5.1), which could cause the delay in myosin II activation and myosin II contractility at the rear. This possibility could be tested by examining the temporal dynamics of MLCK, p160-ROCK and Rho activation in response to attractants, probably with high-sensitivity live cell biosensors for MLCK and p160-ROCK activities. Notably, our findings contrasted an earlier study in which traction stresses were detected mostly in the uropod of neutrophils migrating on a stiffer substrate (9 kPa) (Smith et al., 2007). The differential patterns of tractions observed may be attributed to the differences in substrate stiffness, temporal resolutions of the studies and/or other undefined factors.

On the regulatory mechanisms of traction involving myosin II and its upstream kinases during neutrophil chemotaxis

How are tractions regulated in neutrophils during chemotaxis? Our current findings suggest that tractions at the leading and the trailing edge in neutrophils require myosin II activation. Inhibition of myosin II impairs the level and the periodicity of tractions. Our results suggest that the recruitment of MLCK to the neutrophil's leading edge activates MRLC and myosin II contractility, allowing cells to exert tractions on the ECM substrate, enhance integrin activity and stabilize leading-edge adhesion (Figure 5.1). The spatially controlled activation of Rho, p160-ROCK and subsequent myosin II activation (Xu et al., 2003) leads to contraction of actin-myosin complexes at the trailing edge, causing it to de-adhere (Figure 5.1). At least three possibilities, alone or in combination, could account for the periodic pattern of tractions. It might be that myosin II is activated periodically during chemotaxis. Alternatively, the strength of cell-substrate

adhesion might be temporally regulated, leading to alternation of weak and strong local tractions during neutrophil migration. Third, there might be myosin II-independent mechanism(s) that also contribute to the development and periodicity of tractions. In our experiments, there are significant amounts of tractions remaining after inhibition of total or localization-specific myosin II activities. Our results are in keeping with a recent report demonstrating that inhibition of myosin II functions fails to abolish tractions in *Dictyostelium* cells during chemotaxis (Meili et al., 2010). One group of putative candidates that might control tractions in neutrophils are plasma membrane-anchored myosin class I molecules, which reportedly could generate membrane tension by pulling on F-actin coupled to ECM via integrins (Nambiar et al., 2009). Other candidates include force-bearing cytoskeletal molecules such as microtubules and intermediate filaments that can transmit force to actin through various inter-cytoskeletal linkage (Rodriguez et al., 2003; Wang et al., 2009). More complete understanding of the detailed mechanisms governing the periodic and out-of-phase behavior of tractions awaits future experiments. In addition, future experiments should investigate whether the observed spatiotemporal dynamics of tractions and their regulatory patterns can be extended to neutrophils under other extracellular settings (e.g., on ECM substrates for β2-integrin) and to other amoeboid cells.

MLCK-mediated actomyosin contractility in the regulation of traction, integrin activation and adhesion in neutrophil chemotaxis

In slow migrating cells such as fibroblasts, MLCK is mainly found in stress fibers (Katoh et al., 2001). Distribution of MLCK in neutrophils differs from this pattern. As in neutrophils, MLCK and ROCK in fibroblasts play distinct roles in regulating membrane protrusions and adhesion dynamics during cell migration (Totsukawa et al., 2004a). MLCK inhibition blocks MRLC phosphorylation at the cell periphery, but not in the center and prevents zyxin-containing adhesions at the periphery. These cells generate membrane protrusions all around the cell, turn more frequently, and migrate less effectively. In contrast, ROCK inhibition blocks MRLC phosphorylation in the center and prevents formation of focal adhesions. These cells move faster and straighter. Thus, although the MRLC activation in fibroblasts is spatially controlled by MLCK and ROCK,

their distribution and function in the control of cell migration seem to differ from those in neutrophils.

How might MLCK inhibition (or depletion) at the leading edge affect tractions at both edges in neutrophils during chemotaxis? It is well accepted that organization of actin cytoskeleton in cells is heavily dependent on mechanical force. Increasing tension in the actin network leads to formation of actin bundles, which can be prevented by the inhibition of myosin activity (Amano et al., 1997; Sims et al., 1992). More recently, it was demonstrated that nonmuscle myosin II is required not only to establish but also to maintain integrity of the actomyosin network (Cai et al.). Based on these results, we speculate that the global effect of MLCK inhibition on tractions in neutrophils might be linked to its ability to regulate myosin II-dependent contractility. In this scenario, depletion or inhibition of MLCK impairs myosin II contractility at the leading edge and in turn disrupts the structure and organization of the actin cytoskeleton (Figure 5.1), as shown by experiments with live and fixed neutrophils. Myosin II might crosslink actin filaments into a coherent mechanical network that allows transmission of force from one side of the cell to the other (Sims et al., 1992). In neutrophils, the actin cytoskeletal network appears highly organized and interconnected (Movie S4), and thus might provide a structural framework for the putative mechanotransduction activity. Alternatively, force might be transmitted through connections among different types of cytoskeletons, as shown in other cells and organisms (Petrasek and Schwarzerova, 2009; Rodriguez et al., 2003). Thus, MLCK inhibition at the leading edge could also affect the structure and organization of the actin cytoskeleton at the trailing edge of the cells, leading to a decrease in tractions at the rear. Similarly, this model (Figure 5.1) also explains the decreased tractions at both edges of the cells after p160-ROCK is inhibited.

However, it is of note that the proposed model (Figure 5.1) cannot explain how p160-ROCK-inhibited neutrophils retain periodicity of tractions at both edges on stiffer substrate (100 kPa), while accounting for the reduction in traction level at both edges in the same cells. It might be that a higher-stiffness substrate helps to better support and maintain cytoskeletal organization and integrity in neutrophils, rendering cells less susceptible to local inhibition of myosin II. Indeed, the degree of integrity and organization of actin cytoskeleton is closely related to mechanical properties of

extracellular environment. More bundled, ordered stress fiber formation is observed in fibroblasts on stiffer matrix (Yeung et al., 2005). Furthermore, p160-ROCK, unlike MLCK, is not required for leading edge activities and thus, when inhibited, exerts little effects on leading edge protrusion and stability. As such, the remaining myosin II activity after p160-ROCK inhibition could still enable the cells to maintain the pattern of tractions on both the leading and the trailing edge. An alternative possibility is that the putative myosin II-independent mechanism(s), as discussed earlier, might be actively engaged to support the periodic pattern of tractions at the back of the cells under these conditions.

How does MLCK control integrin activation in neutrophils? Our results, as well as those from others, have begun to point to a role for myosin II-dependent mechanical tension. Friedland *et al.* (Friedland et al., 2009) reported that $\alpha5\beta1$–integrin can switch between relaxed and tensioned states in response to myosin II–generated cytoskeletal force. The resulting force combines with cell-substrate adhesion to generate tension that activates the integrin molecule mechanically. Our results also suggest that myosin II-dependent cellular contraction mediates MLCK's effect on adhesion and integrin activation. MLCK inhibition fails to prevent integrin activation in neutrophils in suspension, implying the role of tractions in the regulation of integrin activity. We suspect that the tension applied to specific molecules (e.g., talin (Tadokoro et al., 2003) or vinculin (Critchley and Gingras, 2008)) that control integrin activity might change their conformations to "active," as in the "conformational switch" model (Geiger and Bershadsky, 2001) proposed to explain the maturation of focal adhesions by internal actin-myosin contraction in fibroblasts. In support of this notion, application of physiologically relevant forces causes stretching of single talin rods that expose cryptic binding sites for vinculin (del Rio et al., 2009). Thus, the documented protein stretching may represent a more general mechanism for force transduction in a variety of signaling events, including integrin activation.

We conclude that periodic, out-of-phase traction generation at the leading and the trailing edges of neutrophils during chemotaxis may be an important mechanism for ensuring persistent movement by coordinating activities at both edges of cells. Future

experiments are necessary to elucidate the molecular mechanisms governing the generation, periodicity, and timing of traction in neutrophil chemotaxis.

Figures

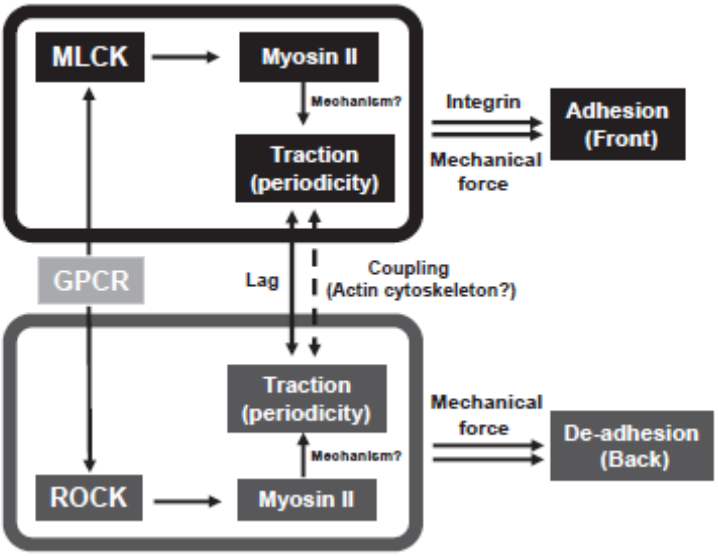

Figure 5.1 Integration of mechanical and biochemical signals to regulate leading edge adhesion and trailing edge de-adhesion: A model.
The model is proposed based on analyses of cell migration on the 3.5 kPa substrate. See text for details. GPCR: G protein-coupled receptor

BIBLIOGRAPHY

Alblas, J., Ulfman, L., Hordijk, P., and Koenderman, L. (2001). Activation of RhoA and ROCK Are Essential for Detachment of Migrating Leukocytes. Mol Biol Cell *12*, 2137-2145.

Amano, M., Chihara, K., Kimura, K., Fukata, Y., Nakamura, N., Matsuura, Y., and Kaibuchi, K. (1997). Formation of Actin Stress Fibers and Focal Adhesions Enhanced by Rho-Kinase. Science *275*, 1308-1311.

Bain, J., McLauchlan, H., Elliott, M., and Cohen, P. (2003). The specificities of protein kinase inhibitors: an update. Biochem J *371*, 199-204.

Balaban, N. Q., Schwarz, U. S., Riveline, D., Goichberg, P., Tzur, G., Sabanay, I., Mahalu, D., Safran, S., Bershadsky, A., Addadi, L., and Geiger, B. (2001). Force and focal adhesion assembly: a close relationship studied using elastic micropatterned substrates. Nat Cell Biol *3*, 466-472.

Ballestrem, C., Hinz, B., Imhof, B. A., and Wehrle-Haller, B. (2001). Marching at the front and dragging behind: differential {alpha}V{beta}3-integrin turnover regulates focal adhesion behavior. J Cell Biol *155*, 1319-1332.

Benard, V., Bohl, B. P., and Bokoch, G. M. (1999). Characterization of Rac and Cdc42 Activation in Chemoattractant-stimulated Human Neutrophils Using a Novel Assay for Active GTPases. J Biol Chem *274*, 13198-13204.

Beningo, K. A., and Wang, Y.-L. (2002). Flexible substrata for the detection of cellular traction forces. Trends in Cell Biology *12*, 79-84.

Bodin, S., and Welch, M. D. (2005). Plasma Membrane Organization Is Essential for Balancing Competing Pseudopod- and Uropod-promoting Signals during Neutrophil Polarization and Migration. Mol Biol Cell *16*, 5773-5783.

Cai, Y., Rossier, O., Gauthier, N. C., Biais, N., Fardin, M. A., Zhang, X., Miller, L. W., Ladoux, B., Cornish, V. W., and Sheetz, M. P. Cytoskeletal coherence requires myosin-IIA contractility. J Cell Sci *123*, 413-423.

Condeelis, J. (1993). Life at the leading edge: the formation of cell protrusions. Annu Rev Cell Biol *9*, 411–444.

Critchley, D. R., and Gingras, A. R. (2008). Talin at a glance. Journal of Cell Science *121*, 1345-1347.

del Rio, A., Perez-Jimenez, R., Liu, R., Roca-Cusachs, P., Fernandez, J. M., and Sheetz, M. P. (2009). Stretching Single Talin Rod Molecules Activates Vinculin Binding. Science *323*, 638-641.

Dembo, M., and Wang, Y.-L. (1999). Stresses at the Cell-to-Substrate Interface during Locomotion of Fibroblasts. Biophys J *76*, 2307-2316.

DiMilla, P. A., Barbee, K., and Lauffenburger, D. A. (1991). Mathematical model for the effects of adhesion and mechanics on cell migration speed. Biophysical journal *60*, 15-37.

Engler, A., Bacakova, L., Newman, C., Hategan, A., Griffin, M., and Discher, D. (2004). Substrate Compliance versus Ligand Density in Cell on Gel Responses. Biophys J *86*, 617-628.

Fechheimer, M., and Zigmond, S. H. (1983). Changes in cytoskeletal proteins of polymorphonuclear leukocytes induced by chemotactic peptides. Cell Motil *3*, 349-361.

Friedl, P. (2004). Prespecification and plasticity: shifting mechanisms of cell migration. Curr Opin Cell Biol *16*, 14-23.

Friedl, P., Zänker, K. S., and Bröcker, E.-B., (1998). Cell migration strategies in 3-D extracellular matrix: Differences in morphology, cell matrix interactions, and integrin function. Microscopy Research and Technique *43*, 369-378.

Friedland, J. C., Lee, M. H., and Boettiger, D. (2009). Mechanically Activated Integrin Switch Controls {alpha}5{beta}1 Function. Science *323*, 642-644.

Fumagalli, L., Zhang, H., Baruzzi, A., Lowell, C. A., and Berton, G. (2007). The Src Family Kinases Hck and Fgr Regulate Neutrophil Responses to N-Formyl-Methionyl-Leucyl-Phenylalanine. J Immunol *178*, 3874-3885.

Geiger, B., and Bershadsky, A. (2001). Assembly and mechanosensory function of focal contacts. Current Opinion in Cell Biology *13*, 584-592.

Geiger, B., and Bershadsky, A. (2002). Exploring the Neighborhood: Adhesion-Coupled Cell Mechanosensors. Cell *110*, 139-142.

Gomez-Mouton, C., Lacalle, R. A., Mira, E., Jimenez-Baranda, S., Barber, D. F., Carrera, A. C., Martinez, A. C., and Manes, S. (2004). Dynamic redistribution of raft domains as an organizing platform for signaling during cell chemotaxis. J Cell Biol *164*, 759-768.

Grinnell, F. (1994). Fibroblasts, myofibroblasts, and wound contraction. J Cell Biol *124*, 401-404.

Gupta, N., and DeFranco, A. L. (2003). Visualizing lipid raft dynamics and early signaling events during antigen receptor-mediated B-lymphocyte activation. Mol Biol Cell *14*, 432-444.

Hauert, A. B., Martinelli, S., Marone, C., and Niggli, V. (2002). Differentiated HL-60 cells are a valid model system for the analysis of human neutrophil migration and chemotaxis. The International Journal of Biochemistry & Cell Biology *34*, 838-854.

Hynes, R. O. (2002). Integrins: bidirectional, allosteric signaling machines. Cell *110*, 673-687.

Janmey, P. A., and McCulloch, C. A. (2007). Cell Mechanics: Integrating Cell Responses to Mechanical Stimuli. Annual Review of Biomedical Engineering *9*, 1-34.

Kamm, K. E., and Stull, J. T. (2001). Dedicated myosin light chain kinases with diverse cellular functions. J Biol Chem *276*, 4527-4530.

Kansas, G. S. (1996). Selectins and their ligands: current concepts and controversies. Blood *88*, 3259-3287.

Katoh, K., Kano, Y., Amano, M., Kaibuchi, K., and Fujiwara, K. (2001). Stress fiber organization regulated by MLCK and Rho-kinase in cultured human fibroblasts. American Journal of Physiology - Cell Physiology *280*, C1669-C1679.

Klemke, R. L., Cai, S., Giannini, A. L., Gallagher, P. J., de Lanerolle, P., and Cheresh, D. A. (1997). Regulation of cell motility by mitogen-activated protein kinase. J Cell Biol *137*, 481-492.

Lauffenburger, D. A., and Horwitz, A. F. (1996). Cell Migration: A Physically Integrated Molecular Process. Cell *84*, 359-369.

Laukaitis, C. M., Webb, D. J., Donais, K., and Horwitz, A. F. (2001). Differential Dynamics of {alpha}5 Integrin, Paxillin, and {alpha}-Actinin during Formation and Disassembly of Adhesions in Migrating Cells. J Cell Biol *153*, 1427-1440.

Lombardi, M. L., Knecht, D. A., Dembo, M., and Lee, J. (2007). Traction force microscopy in Dictyostelium reveals distinct roles for myosin II motor and actin-crosslinking activity in polarized cell movement. J Cell Sci *120*, 1624-1634.

Manders, E. M., Stap, J., Brakenhoff, G. J., van Driel, R., and Aten, J. A. (1992). Dynamics of three-dimensional replication patterns during the S-phase, analysed by double labeling of DNA and confocal microscopy. Journal of Cell Science *103*, 857-862.

Maupin, P., Phillips, C. L., Adelstein, R. S., and Pollard, T. D. (1994). Differential localization of myosin-II isozymes in human cultured cells and blood cells. J Cell Sci *107*, 3077-3090.

Meili, R., Alonso-Latorre, B., del Alamo, J. C., Firtel, R. A., and Lasheras, J. C. (2010). Myosin II Is Essential for the Spatiotemporal Organization of Traction Forces during Cell Motility. Mol Biol Cell *21*, 405-417.

Meili, R., and Firtel, R. A. (2003). Two Poles and a Compass. Cell *114*, 153-156.

Munevar, S., Wang , Y., and Dembo, M. (2001). Traction force microscopy of migrating normal and H-ras transformed 3T3 fibroblasts. Biophys J *80*, 1744–1757.

Nambiar, R., McConnell, R. E., and Tyska, M. J. (2009). Control of cell membrane tension by myosin-I. Proceedings of the National Academy of Sciences *106*, 11972-11977.

Oakes, P. W., Patel, D. C., Morin, N. A., Zitterbart, D. P., Fabry, B., Reichner, J. S., and Tang, J. X. (2009). Neutrophil morphology and migration are affected by substrate elasticity. Blood *114*, 1387-1395.

Oliver, T., Lee, J., Jacobson, K. (1994). Forces exerted by locomoting cells. Seminars Cell Biol *5*, 139 -147.

Orr, A. W., Ginsberg, M. H., Shattil, S. J., Deckmyn, H., and Schwartz, M. A. (2006). Matrix-specific Suppression of Integrin Activation in Shear Stress Signaling. Mol Biol Cell *17*, 4686-4697.

Parent, C. A. (2004). Making all the right moves: chemotaxis in neutrophils and Dictyostelium. Current Opinion in Cell Biology *16*, 4-13.

Parent, C. A., Blacklock, B. J., Froehlich, W. M., Murphy, D. B., and Devreotes, P. N. (1998). G Protein Signaling Events Are Activated at the Leading Edge of Chemotactic Cells. Cell *95*, 81-91.

Pelham, R. J., Jr., and Wang, Y.-l. (1999). High Resolution Detection of Mechanical Forces Exerted by Locomoting Fibroblasts on the Substrate. Mol Biol Cell *10*, 935-945.

Pestonjamasp, K. N., Forster, C., Sun, C., Gardiner, E. M., Bohl, B., Weiner, O., Bokoch, G. M., and Glogauer, M. (2006). Rac1 links leading edge and uropod events through Rho and myosin activation during chemotaxis. Blood *108*, 2814-2820.

Petrasek, J., and Schwarzerova, K. (2009). Actin and microtubule cytoskeleton interactions. Curr Opin Plant Biol *12*, 728-734.

Poperechnaya, A., Varlamova, O., Lin, P. J., Stull, J. T., and Bresnick, A. R. (2000). Localization and activity of myosin light chain kinase isoforms during the cell cycle. J Cell Biol *151*, 697-708.

Ridley, A. J. (2001). Rho family proteins: coordinating cell responses. Trends in Cell Biology *11*, 471-477.

Ridley, A. J., Schwartz, M. A., Burridge, K., Firtel, R. A., Ginsberg, M. H., Borisy, G., Parsons, J. T., and Horwitz, A. R. (2003). Cell Migration: Integrating Signals from Front to Back. Science *302*, 1704-1709.

Rodriguez, O. C., Schaefer, A. W., Mandato, C. A., Forscher, P., Bement, W. M., and Waterman-Storer, C. M. (2003). Conserved microtubule-actin interactions in cell movement and morphogenesis. Nat Cell Biol *5*, 599-609.

Rottner, K., Hall, A., and Small, J. V. (1999). Interplay between Rac and Rho in the control of substrate contact dynamics. Current Biology *9*, 640-648, S641.

Ryu, H., Lee, J. H., Kim, K. S., Jeong, S. M., Kim, P. H., and Chung, H. T. (2000). Regulation of neutrophil adhesion by pituitary growth hormone accompanies tyrosine phosphorylation of Jak2, p125FAK, and paxillin. J Immunol *165*, 2116-2123.

Schymeinsky, J., Sindrilaru, A., Frommhold, D., Sperandio, M., Gerstl, R., Then, C., Mocsai, A., Scharffetter-Kochanek, K., and Walzog, B. (2006). The Vav binding site of the non-receptor tyrosine kinase Syk at Tyr 348 is critical for {beta}2 integrin (CD11/CD18)-mediated neutrophil migration. Blood.

Servant, G., Weiner, O. D., Herzmark, P., Balla, T., aacute, Sedat, J. W., and Bourne, H. R. (2000). Polarization of Chemoattractant Receptor Signaling During Neutrophil Chemotaxis. Science *287*, 1037-1040.

Sims, J. R., Karp, S., and Ingber, D. E. (1992). Altering the cellular mechanical force balance results in integrated changes in cell, cytoskeletal and nuclear shape. Journal of Cell Science *103*, 1215-1222.

Sklar, L. A., Omann, G. M., and Painter, R. G. (1985). Relationship of actin polymerization and depolymerization to light scattering in human neutrophils: dependence on receptor occupancy and intracellular Ca++. J Cell Biol *101*, 1161-1166.

Smith, A., Bracke, M., Leitinger, B., Porter, J. C., and Hogg, N. (2003). LFA-1-induced T cell migration on ICAM-1 involves regulation of MLCK-mediated attachment and ROCK-dependent detachment. J Cell Sci *116*, 3123-3133.

Smith, L. A., Aranda-Espinoza, H., Haun, J. B., Dembo, M., and Hammer, D. A. (2007). Neutrophil Traction Stresses are Concentrated in the Uropod during Migration. Biophysical journal *92*, L58-L60.

Srinivasan, S., Wang, F., Glavas, S., Ott, A., Hofmann, F., Aktories, K., Kalman, D., and Bourne, H. R. (2003). Rac and Cdc42 play distinct roles in regulating PI(3,4,5)P3 and polarity during neutrophil chemotaxis. J Cell Biol *160*, 375-385.

Staffan Johansson, G. S., Krister Wennerberg, Annika Armulik, Lars Lohikangas (1997). Fibronectin-Integrin Interactions. Frontiers in Bioscience *2*, 126-146.

Tadokoro, S., Shattil, S. J., Eto, K., Tai, V., Liddington, R. C., de Pereda, J. M., Ginsberg, M. H., and Calderwood, D. A. (2003). Talin Binding to Integrin 흑 Tails: A Final Common Step in Integrin Activation. Science *302*, 103-106.

Tamariz, E., and Grinnell, F. (2002). Modulation of Fibroblast Morphology and Adhesion during Collagen Matrix Remodeling. Mol Biol Cell *13*, 3915-3929.

Tapon, N., and Hall, A. (1997). Rho, Rac and Cdc42 GTPases regulate the organization of the actin cytoskeleton. Current Opinion in Cell Biology *9*, 86-92.

Tolic-Norrelykke, I. M., Butler, J. P., Chen, J., and Wang, N. (2002). Spatial and temporal traction response in human airway smooth muscle cells. Am J Physiol Cell Physiol *283*, C1254-1266.

Totsukawa, G., Wu, Y., Sasaki, Y., Hartshorne, D. J., Yamakita, Y., Yamashiro, S., and Matsumura, F. (2004b). Distinct roles of MLCK and ROCK in the regulation of membrane protrusions and focal adhesion dynamics during cell migration of fibroblasts. J Cell Biol *164*, 427-439.

Verena, N. (2000). A membrane-permeant ester of phosphatidylinositol 3,4,5-trisphosphate (PIP3) is an activator of human neutrophil migration. FEBS letters *473*, 217-221.

Vicente-Manzanares, M., Zareno, J., Whitmore, L., Choi, C. K., and Horwitz, A. F. (2007). Regulation of protrusion, adhesion dynamics, and polarity by myosins IIA and IIB in migrating cells. J Cell Biol *176*, 573-580.

W. Matthew Petroll, L. M. (2003). Direct, dynamic assessment of cell-matrix interactions inside fibrillar collagen lattices. Cell Motility and the Cytoskeleton *55*, 254-264.

Wang, F., Herzmark, P., Weiner, O. D., Srinivasan, S., Servant, G., and Bourne, H. R. (2002). Lipid products of PI(3)Ks maintain persistent cell polarity and directed motility in neutrophils. Nat Cell Biol *4*, 513-518.

Wang, N., Tytell, J. D., and Ingber, D. E. (2009). Mechanotransduction at a distance: mechanically coupling the extracellular matrix with the nucleus. Nat Rev Mol Cell Biol *10*, 75-82.

Webb, D. J., Donais, K., Whitmore, L. A., Thomas, S. M., Turner, C. E., Parsons, J. T., and Horwitz, A. F. (2004). FAK-Src signaling through paxillin, ERK and MLCK regulates adhesion disassembly. Nat Cell Biol *6*, 154-161.

Weiner, O. D., Neilsen, P. O., Prestwich, G. D., Kirschner, M. W., Cantley, L. C., and Bourne, H. R. (2002). A PtdInsP3- and Rho GTPase-mediated positive feedback loop regulates neutrophil polarity. Nat Cell Biol *4*, 509-513.

Weiner, O. D., Rentel, M. C., Ott, A., Brown, G. E., Jedrychowski, M., Yaffe, M. B., Gygi, S. P., Cantley, L. C., Bourne, H. R., and Kirschner, M. W. (2006). Hem-1 complexes are essential for Rac activation, actin polymerization, and myosin regulation during neutrophil chemotaxis. PLoS Biol *4*, e38.

Wilson, A. K., Gorgas, G., Claypool, W. D., and de Lanerolle, P. (1991). An increase or a decrease in myosin II phosphorylation inhibits macrophage motility. J Cell Biol *114*, 277-283.

Wolf, K., Mazo, I., Leung, H., Engelke, K., von Andrian, U. H., Deryugina, E. I., Strongin, A. Y., Brocker, E.-B., and Friedl, P. (2003a). Compensation mechanism in tumor cell migration: mesenchymal-amoeboid transition after blocking of pericellular proteolysis. J Cell Biol *160*, 267-277.

Wolf, K., Muller, R., Borgmann, S., Brocker, E. B., and Friedl, P. (2003b). Amoeboid shape change and contact guidance: T-lymphocyte crawling through fibrillar collagen is independent of matrix remodeling by MMPs and other proteases. Blood *102*, 3262-3269.

Wong, K., Pertz, O., Hahn, K., and Bourne, H. (2006). Neutrophil polarization: spatiotemporal dynamics of RhoA activity support a self-organizing mechanism. Proc Natl Acad Sci U S A *103*, 3639-3644.

Xu, J., Gao, X. P., Ramchandran, R., Zhao, Y. Y., Vogel, S. M., and Malik, A. B. (2008). Nonmuscle myosin light-chain kinase mediates neutrophil transmigration in sepsis-induced lung inflammation by activating beta2 integrins. Nat Immunol *9*, 880-886.

Xu, J., Wang, F., Van Keymeulen, A., Herzmark, P., Straight, A., Kelly, K., Takuwa, Y., Sugimoto, N., Mitchison, T., and Bourne, H. R. (2003). Divergent signals and cytoskeletal assemblies regulate self-organizing polarity in neutrophils. Cell *114*, 201-214.

Yanai, M., Butler, J.P., Suzuki, T., Sasaki, H. and Higuchi, H. (2004). Regional rheological differences in locomoting neutrophils. Am J Physiol Cell Physiol *287*, C603–C611.

Yanai, M., Kenyon, C.M., Butler, J.P., Macklem, P.T. and Kelly, S.M. (1996). Intracellular pressure is a motive force for cell motion in Amoeba proteus. Cell Motil Cytoskeleton *33*, 22-29.

Ydrenius, L., Molony, L., Ng-Sikorski, J., and Andersson, T. (1997). Dual action of cAMP-dependent protein kinase on granulocyte movement. Biochem Biophys Res Commun *235*, 445-450.

Yeung, T., Georges, P.C., Flanagan, L.A., Marg, B., Ortiz, M., Funaki, M., Zahir, N., Ming, W., Weaver, V., and Janmey, P.A. (2005). Effects of substrate stiffness on cell morphology, cytoskeletal structure, and adhesion. Cell Motility and the Cytoskeleton *60*, 24-34.

Zamir, E., Katz, M., Posen, Y., Erez, N., Yamada, K. M., Katz, B.-Z., Lin, S., Lin, D. C., Bershadsky, A., Kam, Z., and Geiger, B. (2000). Dynamics and segregation of cell-matrix adhesions in cultured fibroblasts. Nat Cell Biol *2*, 191-196.

Zarbock, A., and Ley, K. (2009). Neutrophil Adhesion and Activation under Flow. Microcirculation *16*, 31-42.

Zhelev, D. V., Alteraifi, A. M., and Chodniewicz, D. (2004). Controlled pseudopod extension of human neutrophils stimulated with different chemoattractants. Biophys J *87*, 688-695.

APPENDIX:
TEXT FOR SUPPLEMENTARY MOVIES

Supplementary Movie S1 (traction map) shows the responses of control dHL-60 cells to a point source of fMLP. Some of the time points are shown in Figure 2.1A in the text. The total time is 290 sec.

Supplementary Movie S2 (fluorescence channel) and Supplementary Movie S3 (DIC channel) show the responses of dHL-60 cells expressing mCherry-tagged myosin IIA to a point source of fMLP. Some of the time points are shown in Figure 3.1B in the text.

Supplementary Movie S4 (green fluorescence channel) and Supplementary Movies S5 (red fluorescence channel) show 3 dimensional views of a polarized dHL-60 cell stained with Alexa fluor 488 phalloidin to localize F-actin (green; Movie S4) and a specific antibody against myosin IIA (red; Movie S5). The schematic views are shown in Figure 3.1D.

Supplementary Movie S6 (DIC channel) shows the responses of control dHL-60 cells to a point source of fMLP. Some of the time points are shown in Figure 3.4A in the text.

Supplementary Movie S7 (DIC channel) shows the responses of blebbistatin-treated dHL-60 cells to a point source of fMLP. Some of the time points are shown in Figure 3.4A in the text.

Supplementary Movie S8 (DIC channel) shows the responses of myosin IIA-depleted dHL-60 cells to a point source of fMLP. Some of the time points are shown in Figure 3.4A in the text.

Supplementary Movie S9 (DIC channel) shows the responses of Y-27632-treated dHL-60 cells to a point source of fMLP. Some of the time points are shown in Figure 3.4A in the text.

Supplementary Movie S10 (GFP channel) and Supplementary Movie S11 (DIC channel) show the responses of dHL-60 cells expressing sMLCK-EGFP to a uniform concentration of fMLP. Some of the time points are shown in Figure 4.1D in the Supplementary Information.

Supplementary Movie S12 (traction map) shows the responses of MLCK-depleted dHL-60 cells to a point source of fMLP. Some of the time points are shown in Figure 4.8A in the text. The total time is 290 sec.

CURRICULUM VITAE

Myung Eun Shin

Department of Cell and Developmental Biology
University of Illinois at Urbana-Champaign
B520 Chemical and Life Sciences Laboratory
601 S. Goodwin Avenue
Urbana, IL 61801

EDUCATION

Ph.D. in Cell and Developmental Biology 2011
University of Illinois at Urbana-Champaign

B.S. in Biological Sciences 2005
Ewha Womans University, Korea

Exchange Student 2003-2004
University of Wisconsin, Madison

RESEARCH EXPERIENCE

2005-Present **Dept. of Cell and Developmental Biology**
University of Illinois at Urbana-Champaign
Doctoral research in the laboratory of Dr. Fei Wang.
Dissertation title: The spatiotemporal organization, regulation, and function of tractions during neutrophils chemotaxis

2004-2005 **Dept. of Biological Sciences**
Ewha Womans University
Research assistant in laboratory of Dr. Chang-Yeol Yeo
Project: The role of SMAD4 in the embryonic development of the *Xenopus laevis*

2004 **Dept. of Biological Sciences**
Ewha Womans University
Research assistant in laboratory of Dr. Gootaek Oh
Project: The function of annexin A2 in cardiovascular diseases.

2003 **Dept. of Biological Sciences**
Ewha Womans University
Research assistant in laboratory of Dr. Wonja Choi
Project: The involvement of gene Pra1 in adaptive oxidative stress response of *Candida albicans*

PUBLICATIONS

Li, D., Zhou, J., Wang, L., **Shin, M.E.**, Su, P., Lei, X., Kuang, H., Guo, W., Yang, H., Cheng, L., Tanaka, T.S., Leckband, D.E., Reynolds, A.B., Duan, E., and Wang, F. (2010). Integrated biochemical and mechanical signals regulate multifaceted human embryonic stem cell functions. *J. Cell Biol.* 191(3): p. 631–644.

Shin, M.E., He, Y., Li, D., Na, S., Chowdhury, F., Poh, Y.C., Collin, O., Su, P., de Lanerolle, P., Schwartz, M.A., Wang, N., and Wang, F. (2010) Spatiotemporal organization, regulation, and functions of tractions during neutrophil chemotaxis. *Blood,* 116 (17): p. 3297-3310.

Collin, O., Na, S., Chowdhury, F., Hong, M., **Shin, M.E.**, Wang, F., and Wang, N. (2008) Self-Organized Podosomes Are Dynamic Mechanosensors. *Current Biology*, 18(17): p.1288-1294.

Chen, S., Lin, F., **Shin, M.E.**, Wang, F., Shen, L., and Hamm, H.E. (2008). RACK1 Regulates Directional Cell Migration by Acting on Gβγ at the Interface with its Effectors PLCβ and PI3Kγ. *Mol Biol Cell*, 19(9): p. 3909-3922.

HONORS AND AWARDS

2005 Doctoral Oversees Scholarship (Korean Foundation for Advancement of Studies))
2004 Dean's List (University of Wisconsin-Madison)
2002 Dean's List (Ewha Womans University)

TEACHING EXPERIENCE

2009 University of Illinois at Urbana-Champaign
Graduate Teaching Assistant for MCB 405: Genetics and Genomics

2009 University of Illinois at Urbana-Champaign
Graduate Teaching Assistant for MCB 151: Molecular and Cellular Biology Laboratory